EXPERT REVIEW

Comprehensive review on design perspective of PET ligands based on β-amyloids, tau and neuroinflammation for diagnostic intervention of Alzheimer's disease

Parul Mittal[1,2] · Niharika Singh[1] · Shubhra Chaturvedi[1] · Amar Jyoti[2] · Anil K. Mishra[1] · Puja Panwar Hazari[1]

Abstract

Purpose Alzheimer's disease (AD) is a progressive neurodegenerative pathological condition that resulted from the deterioration of cholinergic neurons over time. The pathological hallmark features of AD include extracellular β-amyloids plaques, hyperphosphorylated τ protein (tau), which is the main component of neurofibrillary tangles (NFT) and neuroinflammation. This article aims to provide a comprehensive review of PET tracers for Alzheimer's disease, focusing on developments for targets (β-amyloids, hyperphosphorylated τ protein (tau), neuroinflammation and other related targets) available for clinical PET imaging.

Methods/design Studies involving the existing PET tracers used in the imaging of Aβ, tau, and neuroinflammation with essential features and limitations are discussed. Experimental studies with the design perspective of PET tracers, for biomarkers like Aβ, tau protein, and neuroinflammation, which are exploited clinically through PET Imaging have been described in detail. Comparative data have been generated based on the strength and weakness of PET radioligands for preclinical and clinical studies based on their binding affinity, selectivity and imaging. PET tracers for other targets like cannabinoid receptor type 2 (CB2), P2X7 receptor, cyclooxygenase-2, macrophage colony-stimulating factor 1 receptor (CSF1R), and monoamine oxidase (MAO) have also been included.

Result We have summarized the ideal properties in terms of tracer's design for each target and based on their target selectivity and affinity, considering its potential strength and limitations. Where multiple tracers were present for a target, we provide a comparison of their properties. A critical assessment of both the preclinical and clinical PET tracers is carried out where sufficient data are available. This can help in designing better and highly selective PET tracers.

Conclusion Our comprehensive review will provide comparison and help in the design perspective of the futuristic PET tracers for Alzheimer's disease by improving their affinity towards biomarkers with higher selectivity Aβ/tau for delineation of AD at an early stage.
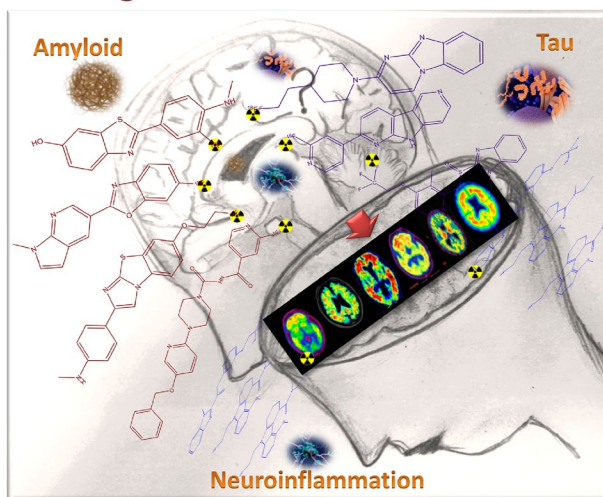
✉ Puja Panwar Hazari
    puja.hazari@gmail.com; puja@inmas.drdo.in

1   Divison of Cyclotron and Radiopharmaceutical Sciences,
    Institute of Nuclear Medicine and Allied Sciences, Brig. SK
    Mazumdar Road, Timarpur, Delhi 110054, India

2   Department of Zoology, Delhi University, Delhi 110007,
    India

Graphic abstract

Introduction

Neurocognitive disorders (NCDs) are marked by impairments in cognitive abilities, including loss of memory, emotional behavior, personality skills, difficulty in solving problems, language, and perception. NCDs commonly result from disturbances in the neural pathways leading to Alzheimer's, Parkinson's, and many other cognitive disorders. Alzheimer's disease (AD) accounts for about 60–70% of neurocognitive disorders [1]. There are various risk factors associated with AD, such as age, diabetes, neuroinflammation in the brain, obesity, and brain injury. With aging, chronic inflammation in the brain increases the risk factor for the development of AD [2]. National Institute of Aging and the Alzheimer's Disease Association has classified AD into three stages: preclinical AD, mild cognitive impairment (MCI), and dementia [3]. Dementia is the main cause of Alzheimer's disease, associated with misfolding of proteins and aggregation at the molecular level, mitochondrial abnormalities, oxidative stress, and neuroinflammation [3]. AD is driven by the deposition of β-amyloid plaques and intracellular accumulation of abnormally hyperphosphorylated tau proteins. The current diagnosis of AD is based on disease history, clinical manifestations, and psychological tests and imaging. Neuroimaging plays a vital role in the diagnosis of AD using multimodal imaging like MRI and PET. PET imaging provides metabolic and molecular information of the brain; whereas, MR imaging gives structural and functional information of the brain. PET Imaging has a high sensitivity in detecting the amyloid plaques, distribution of tau

lesions, and neuroinflammation in AD. β-amyloid plaques are the extracellular deposits of small polypeptide β-amyloid protein generated by processing of β-amyloid precursor protein (APP), a larger transmembrane protein, by the successive action of proteolytic enzymes such as secretases. Tau is an unfolded protein belonging to the microtubule-associated protein (MAP) family of proteins. Tau binds to tubulin protein and stabilizes it, and controls the polymerization of microtubules. Under physiological conditions, post-translation modifications play a significant role in the normal functioning of a protein. One such abnormality is found in the phosphorylation of tau in AD. In the hyperphosphorylated state, tau protein starts pairing with other tau threads to form paired helical filaments (PHF) and tangle together which caused microtubule disintegration. Neurofibrillary tangles (NFTS) are aggregates of microtubule-associated hyperphosphorylated tau (P-tau) are the primary marker in the AD known to cause taupathies [4].It also leads to the formation of extremely insoluble aggregates of tau and the collapse of the neuronal transport system [5]. Since Aβ-plaques and NFTs share a similar β-sheet structure, there are structural similarities present in the imaging agents for both species. For ligand discovery, compound screening approaches were utilized, stating that fused aromatic systems are more likely to interact with the β-sheet fibrillar aggregates. Compound screening is based on competitive in vitro assays using either synthetic heparin-induced tau polymers (HITP) or post-mortem AD human brain homogenates (ADPHFs) or sections. HTIP has not been successful for identifying ligands; so,

assays based on AD brain homogenates have yielded the most promising ligands [6].

The diagnosis of AD requires histological examination of the post-mortem brain sample, but in living patients, CSF biomarkers, PET (Positron emission tomography), CT scan, and MRI are performed. Measurement of Aβ proteins and tau proteins level in the CSF is also a tool in the diagnosis of the disease. Though measuring of proteins in CSF is an invasive method of evaluation with less expense but it may cause several side effects. Non-invasive techniques are used to identify people who are at the risk of developing AD, or the progression of the disease. PET is more widely used than any other technique because it can detect a picomolar concentration of high-affinity molecular probes in the brain which is utilized to visualize an image, characterize and quantify physiological activity at a molecular- and cellular level [7]. Before the advent of highly selective amyloid PET radiotracer for imaging of AD, FDG was used for its detection, but the accuracy was age dependent, and it opened the avenue for the development of newer radiotracers for AD.

Evaluation of brain amyloidosis and neurodegeneration is made possible in a single scan simultaneously through the dual-phase amyloid PET scan. A sharp image is acquired of about 5 min immediately post-injection. This amyloid PET scanning has already been tested with [^{11}C]-PIB and [^{18}F] Florbetapir, revealing high lipophilicity of amyloid tracers, making them good perfusion surrogates. There are several advantages of dual-phase approach, such as less radiation dose, cost-effectiveness, and investigation of neuronal injury and molecular pathology simultaneously based on a single scan rather than two separate scans [8]. This approach is less time consuming and limits the efforts of healthcare workers and patients [9].

In search of new PET tracers, thioflavin-T (Th-T) and congo red were exploited, which have been used as conjugated dyes for staining of plaques and tangles in postmortem AD brain. The development of amyloid-specific and tau imaging compounds is based mostly on the structure of these staining compounds. Various derivatives were synthesized based on Congo red dye, showed nanomolar binding affinity to amyloid and tau aggregates, but they ionize at physiological pH and unable to achieve high brain uptake (> 1 SUV) a few minutes post intravenous injection. The derivatives of Th-T derivatives were made through neutralizing the dye by the removal of the methyl group attached to the benzothiazole ring via the nitrogen atom of the ring, hence giving the positive charge on the benzothiazole ring, which gave rise to compounds known as benzothiazole anilines or BTAs with improved lipophilicity. Another imaging tracer, [^{11}C]PiB was made by modulation of benzothiazole ring by derivatizing the C6 position and varying the degree of methylation of the aniline nitrogen [10]. The success of PiB for in vivo imaging of Aβ plaque deposition led to the development of other tracers based on ^{18}F considering the limitations of ^{11}C isotope.

Compound screening for tau imaging agents led to the discovery of leads based on quinolines, benzimidazoles, benzothiazoles, benzoxazoles, and naphthalene. In 2005, Okamura et al. tested over 2000 molecules for the discovery of PET tracer targeting tau aggregates. This resulted in the discovery of quinolines and benzimidazoles leads such as BF-158, BF-170, and BF-126, which showed low affinity and selectivity for tau aggregates. BF-126 resembles [^{11}C] PIB, with the benzothiazole core being replaced by benzimidazole and a carbon–carbon double-bond spacer being inserted between the planar aromatic ring and the aniline-like substituent at position 2. In 2007, Kuret et al. campaigned another screening of compounds aiming for high affinity to tau aggregates and less to amyloid plaques. This led to the identification of phenyldiazenyl benzothiazole (PDB) derivative having twofold selectivity for tau tangles over amyloid. In this, PDB derivative resembles BF-126 structurally; a benzimidazole replaces benzothiazole and a diazo group the carbon–carbon double bond. Structural modification of BF-170 gave [^{18}F]THK-523, a [^{18}F]fluoroethoxy derivative made by the introduction of an alkyl ether in the C6 position of the arylquinoline structure. This has improved its affinity and selectivity for tau aggregates relative to BF-170 [6].

The translocator protein (TSPO), originally named as the peripheral benzodiazepine receptor, is a neuroinflammation biomarker. TSPO as a ligand, has been used for PET imaging in various animal models for neuroinflammatory conditions such as AD. Using [^{11}C]PK 11195, the first-generation radioligand high TSPO PET brain signal was observed in AD; whereas, no difference in TSPO PET signal was found using second-generation ligands like PBR-28. The clinical trials failed because of high inter-individual variability in the PET signal. PBR-28, DPA-713, and DAA1106, second-generation ligands, showed three different binding patterns in tissue from human donors [11]. The presence of single nucleotide polymorphism (SNP) in the TSPO gene predicted the binding affinity distribution. This rs6971 SNP causes a non-conservative substitution of alanine for threonine at the 147th amino acid (A147T) of TSPO [12]. Considering the facts stated above has led to the development of novel precursors having a minimal genetic predisposition, which are discussed later.

A critical point for the progress in PET tracers includes the development of different radiopharmaceuticals such as ^{11}C, ^{18}F, and ^{68}Ga. ^{68}Ga is a positron emitter with a half-life ($T_{1/2}$) of 67.7 min more prolonged than the half-life of ^{11}C and less than ^{18}F. Considering the advantage of using ^{68}Ge/^{68}Ga generators is the long half-life of the ^{68}Ge/^{68}Ga generator system, which is 270 days. Consequently, multiple elutions are possible every day from this generator [13].

Also, the cost of ^{68}Ga is much reduced as there is no need for an on-site cyclotron. Similarly, ^{18}F also does not require on-site cyclotron; whereas, there is a requirement of on-site cyclotron and expertise in carbon-11 radiochemistry.

This review focuses on the design perspective of PET radiotracers developed so far, covering Alzheimer's Disease pathology with their potential features along with the limitations for the diagnosis of these biomarkers of AD.

Relationship between AChE, β-amyloid plaque and tau protein as a potential target for Alzheimer's disease diagnosis

AChE is a key enzyme in the cholinergic nervous system, its profound loss leads to the progression of Alzheimer's and decreases the levels of acetylcholine in the brain. During the progression of this disease, two more pathological features are responsible for affecting levels of AChE in the brain. β-amyloid plaques (Aβ peptides) and tau protein are two such pathological hallmarks that are found to be associated with the activity of the AChE enzyme. There is the formation of Aβ peptides by the successive proteolytic actions of β-secretase and γ-secretase enzymes on APP resulting in presenilin-1 (PS-1) protein as an active component given on cleavage of the γ-secretase enzyme. Aβ deposition is caused by a mutation in this gene PS-1, which is in turn modulated by AChE. Overexpression of the AChE level can influence the PS-1 level, which forms Aβ plaques in the brain. Also, AChE levels can be influenced by Aβ peptides resulting in an increased level of enzyme around the plaques. Also, increased activity of AChE can activate tau kinase GSK-3β, which can initiate phosphorylation of tau protein [4]. Aβ deposition decreases the production of acetylcholine and increases the activity of AChE around the plaques, and prevents axonal transport and causes excitotoxicity [14]. On the other hand, AChE acts as a chaperone, which induces Aβ aggregates and forms binding sites with Aβ molecules at PAS of enzyme and, thus, increases neurotoxicity in the brain [15]. Dysregulation of APP metabolism leads to amyloid plaques, which worsen the tau aggregation inside the neurons. This is explained by the impairment in APP metabolism, which increases the level of APP C-terminal fragment and leads to synaptic and axonal defects along with the dissociation of tau proteins. Thus, the failure of APP metabolism is responsible for both tau aggregation and Aβ amyloidosis. This further worsens the condition of Alzheimer's by causing oxidative stress, apoptosis, mitochondrial dysfunction, neuronal damage by neuroinflammation. In normal conditions, the Wnt signaling pathway is involved in the modulation of tau phosphorylation and APP production. Dysregulation of this Wnt pathway disrupts glucose metabolism in the brain along with the dysfunction of apolipoprotein E protein, which further dysregulates amyloid and tau pathologies [16]. This shows Aβ and tau act in parallel and synergistically targeting cellular processes. These pieces of evidence give a interrelated pathway of AChE, Aβ, and tau protein affecting each other in different ways and act as potential targets for the diagnosis of AD (Fig. 1).

Pre-requisites of PET ligands for diagnosis of AD in nuclear medicine

PET probes should meet below-mentioned criteria to be used in the diagnosis of neurocognitive disorders by providing information about the disease pathology through non-invasive brain imaging. For brain imaging, visualization of cellular functions and metabolic processes is a must. For this, two types of imaging probes could be utilized; (1) passive agents—modulating an external signal as in US and CT; (2) use of probes that can produce a signal (radiotracer/bioluminescent dyes) or transform an external signal as in PET and MRI.

CT requires a very high concentration of contrast agents; whereas, radiotracers can be detected at high sensitivity [17].
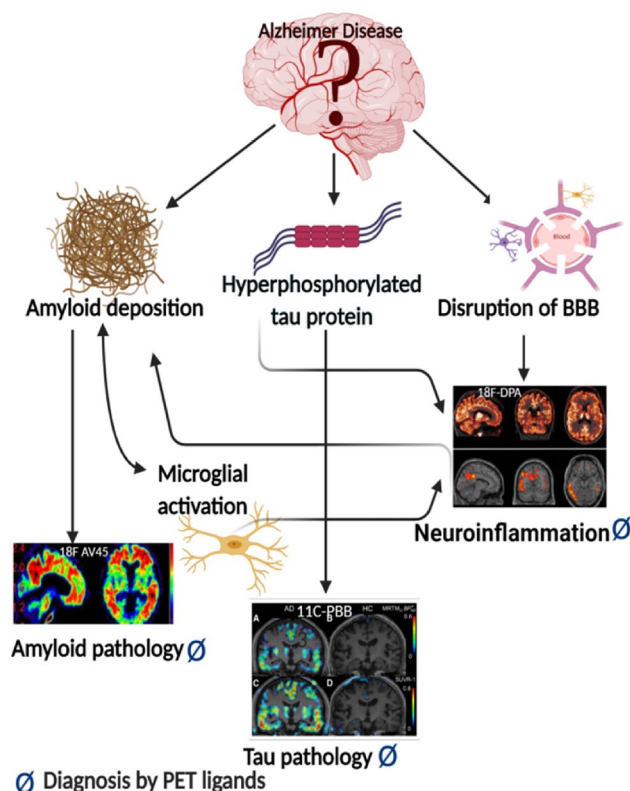
Fig. 1 Schematic representation showing potential targets for the detection of Alzheimer disease at different pathophysiological state [Image created by biorender.com]

The preclinical stage usually starts years or decades ago, where patients do not show any symptoms in cerebral amyloidosis. In the first stage of the preclinical phase, there is the beginning of aggregation of monomeric Aβ, leaving their reservoir in CSF and starting phase of accumulation on the synapses and neuronal surface, which is not even detectable by these advance modalities. Whereas in the second stage of the preclinical phase, there is an increase in CSF tau along with the hypometabolism in the posterior cingulate and cortical thinning which becomes detectable [14].

An ideal radioligand should fulfill the following criteria for becoming a successful ligand for brain imaging by PET:

1. The radiotracer should have high brain penetration capability by passive diffusion so that it can cross BBB, cell membrane, and can enter neurons [18].
2. High specific activity radiolabel allowing high target to non-target ratio.
3. It should not be a P-glycoprotein substrate.
4. It should be of small molecular weight (< 700 Da).
5. Favorable pharmacokinetics for PET imaging, lacking radioactive metabolites which can cross the blood–brain barrier.
6. It should have moderate lipophilicity 1–3 with physiological pH of 7.4, k_d value in the range of 1 nM (long enough for binding of radioligand to amyloid or tau).
7. For developing a radioligand, target selectivity and specific binding are the essential parameters. They should reversibly bind to targets in the brain with high affinity.
8. Short-lived radiotracer should have a standard uptake value (SUV) > 1.0 within a few minutes of intravenous injection in the brain [10].

Jack et al. [5] proposed a classification scheme for AD biomarkers, i.e., "A/T/N" system. In this system, biomarkers of AD are classified into three categories based on the nature of the pathophysiology that each measure. "A" refers to the amyloid-beta biomarker (amyloid PET or CSF Aβ42), "T" is for tau biomarker (CSF phosphorylated tau or tau PET), whereas "N" is a biomarker for neuronal injury or neurodegeneration.

FDG as initial PET tracer for AD

2-Deoxy-2-[18F]fluorodeoxyglucose/([18F]FDG):Initially, 2-Deoxy-2-[18F] fluorodeoxyglucose ([18F] FDG) was utilized as PET agent for imaging. It is a glucose analog that is easily taken up by healthy brain cells due to the high metabolism of glucose, whereas there is less uptake of [18F] FDG due to the slow metabolism of glucose in people affecting from AD [19]. It can detect the functional changes in the brain in healthy individuals, which can be at risk of AD. The use of this compound was efficient for imaging and diagnosis

of AD, but the accuracy of the scan was found to be dependent on the age of the individual. Studies showed 100% sensitivity and 75% specificity in the younger cohort(mean age as 64 years); whereas, this specificity was 20% less than the younger cohort for older patients [20]. [18F]-FDG PET studies revealed reduced glucose metabolism in the parietotemporal, frontal, and posterior cingulate cortices of patients with AD compared with healthy individuals. Also, these decreases are correlated with the severity of dementia [21] (Fig. 2). Altered biodistribution of [18F] FDG and fasting blood glucose level of patients also influence the measured glucose uptake level in the patient [20]. Though FDG PET and MRI are considered less accurate as diagnostic tools due to their low specificity in the detection of amyloidosis and other biomarkers, they are able to correlate with clinical severity, particularly hippocampal atrophy assessed by MRI,
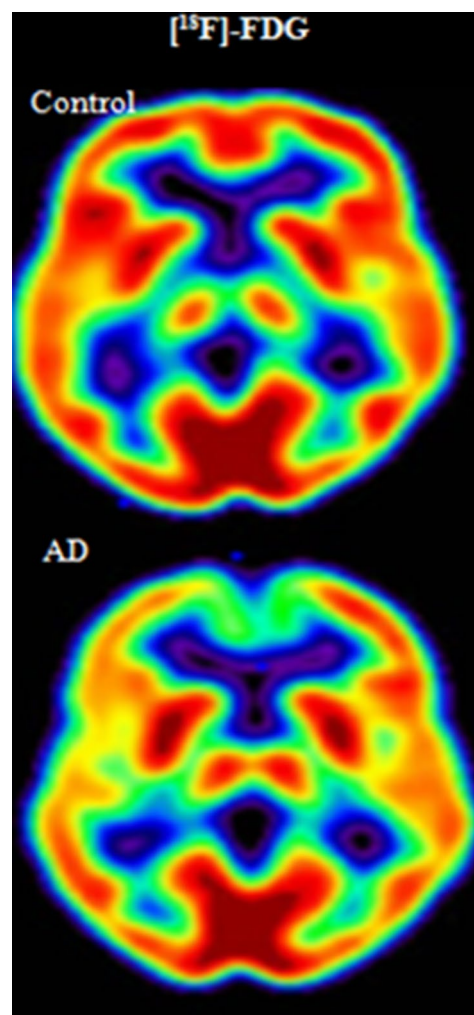

Fig. 2 PET scan depicting deficits in glucose metabolism due to low uptake of 18F-FDG in the parietotemporal cortices of the right hemisphere [23]

cortical hypometabolism measured by FDG PET. Thus, these downstream topographical markers are considered better in monitoring the course of AD (IWG-2 Criteria) [22].

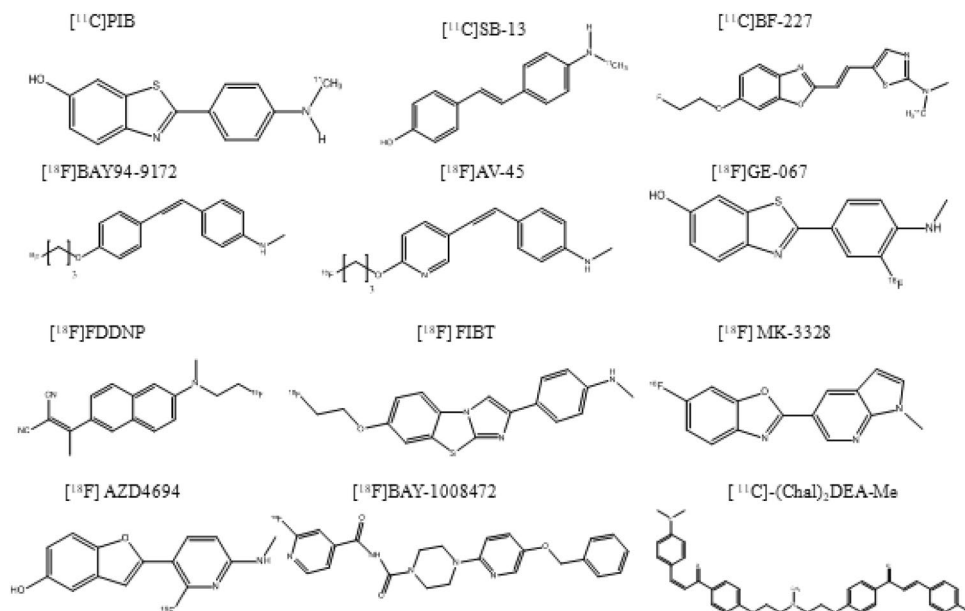## ([^{18}F]-FDDNP): a dual marker for amyloid and tau aggregation Imaging

2-(1-(6-[(2-^{18}F-fluoroethyl)(methyl)amino]-2-naphthyl) ethylidene)malononitrile ([^{18}F]-FDDNP)

In 1999, Barrio and associates attempted to visualize AD in the brain of living human using PET imaging [24]. The ^{18}F-labeled PET tracer developed was
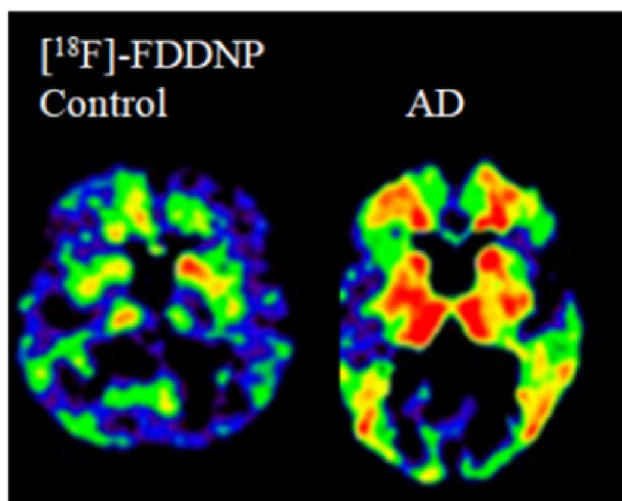
Fig. 3 [^{18}F]FDDNP PET images in healthy control and AD patient showing a high level of [^{18}F]FDDNP binding in subcortical structures suggesting non-specific binding [27]

2-(1-(6-[(2-^{18}F-fluoroethyl)(methyl)amino]-2-naphthyl) ethylidene)malononitrile ([^{18}F]FDDNP) which allowed in vivo measurement of both amyloid and tau aggregation in human brain. But it was found that [^{18}F]FDDNP has a binding affinity to both amyloid and tau aggregates, which made it less specific for evaluation of tau pathology [25, 26]. Preclinical or early detection of AD pathology in living humans at its onset is possible using FDDNP because of its sensitivity for tau aggregates. Imaging with FDDNP gives minimal cortical differences between AD subjects and control. Also, FDDNP shows the lowest level of a signal in the medial temporal region, which is the cortical area for the earliest pathology of disease, and this limits the use of this tracer [24] (Fig. 3).

PET ligands for diagnosis of amyloid-beta plaques

There are various radiotracers developed for PET scan of Aβ imaging as it was the first target and most studied for the neuroimaging of AD (Fig. 4).

First-generation of amyloid PET tracers

Pittsburgh compound-B ([^{11}C]PiB)

In 2004, the first human amyloid PET study was published by Klunk et al. using ^{11}C-labeled Pittsburgh compound-B ([^{11}C]PiB). [^{11}C]PiB was the first carbon-11-labeled tracer studied. [^{11}C]PiB is also known as N-methyl-[^{11}C]2-(4′-methylaminophenyl)-6-hydroxybezothiazole, a derivative of an amyloid binding dye thioflavin-T [28]. It was the most validated tracer which binds to aggregated, fibrillary Aβ

Fig. 4 Chemical structures of β-amyloid plaques targeting PET imaging agents in AD patients

deposits found in the cerebral cortex and striatum but did not bind to amorphous Aβ deposits. Modification of thioflavin T dye gives benzothiazoles, which has a high affinity for binding to amyloid and can cross BBB as well. There were various derivatives of benzothiazole which could bind to amyloid at nanomolar concentration and can enter the brain to give imaging by PET. Based on SAR studies of series of benzothiazole derivatives, PIB (hydroxylated BTA-1 derivative) was considered as the lead compound due to its rapid brain clearance property in rodents and non-human primates [29]. This compound was named on center code 'Pittsburgh Compound-B or PIB' of Uppsala University, where it was evaluated for clinical studies [30].

Preclinical studies were performed in baboons and mice showing fast brain uptake and rapid clearance of radiotracer. Studies showed uniform distribution of the tracer in the baboon brain. The peripheral metabolism PIB in control mice was rapid, with unmetabolized tracer comprising $73 \pm 12\%$ of total plasma radioactivity at 2 min post-injection and $6.4 \pm 2.0\%$ at 30 min. PIB possessed a relatively high 2 min-to-30 min ratio of 11, indicating an in vivo clearance half-life of this compound of approximately 6 min from a normal mouse brain. The radiolabeled metabolites were polar and had low brain uptake. It has a high binding affinity (K_i and K_d values were in the range of 2–4 nM) to aggregated synthetic Aβ(1–40) and Aβ(1–42) fibrils and Aβ plaques in human AD brain tissues and has a very low affinity to NFTs [28]. In vivo brain uptake and clearance studies with PIB in baboons revealed favorable pharmacokinetics with respect to the rapid clearance of radiotracer from healthy non-human primate brain. Autoradiographic studies of post-mortem brain tissue with PIB showed specific and displaceable binding to AD cortical areas containing amyloid deposits, but not to the control cortex. These studies are consistent with metabolic data in mice showing rapid plasma metabolism and the nature of metabolites as polar with the least entry into the brain [29]. Histopathological studies demonstrated the absence of non-specific binding to cerebellar tissues in the postmortem AD brain, suggesting a low density of amyloid plaques in the cerebellum. AD patients showed extensive retention of [11C]PiB in the cortex regions, which contain a substantial amount of Aβ plaques when compared to the healthy individuals. The most important criterion for a successful PET tracer is the rapid clearance of tracer from the brain, which was fulfilled by [11C] PIB. But due to the short half-life (20.3 min) and high cost of the [11C]PiB and the need for in-house cyclotron, its use was limited and soon was replaced by other compounds [5, 10, 20] (Figs. 5a, 6a; Table 1).

[11C]SB-13

[3H]SB-13 is the third PET radioligand tested in humans after FDDNP and 11C-PIB.

Fig. 5 Preclinical amyloid PET images of APP/PS1 transgenic animals are shown in **a** [11C] PiB[39], **b** [18F]AV-45 [45] in rhesus monkey, **c** [18F]Florbetaben [39] and **d** [18F]FIBT [39] in APP/PS1 transgenic animals, **e** [18F]BAY1008472 [44] and **f** [18F]MK-3328, [18F]AD-269, [18F]AD-278, [18F]AD-265[45], showing the distribution in the rhesus monkey. FIBT showed better pharmacokinetic profile and specific binding affinity to Aβ than florbetaben in transgenic mice
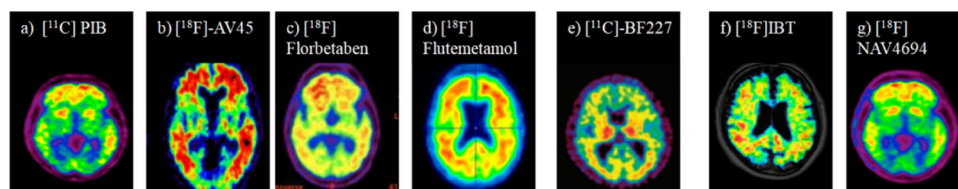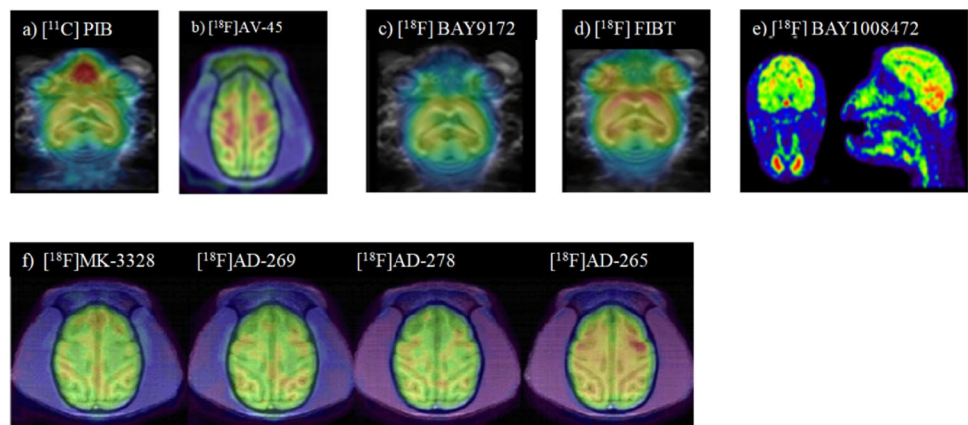
Fig. 6 PET images of amyloid tracers showing distribution in AD patients. **a** [11C]PiB[43], **b** [18F]-AV-45 [46], **c** [18F]Florbetaben [46], **d** [18F] Flutemetamol [37], **e** [11C]BF227[38], **f** [18F]FIBT [40], **g** [18F]NAV4694 [43]

Table 1 PET amyloid radioligands for the diagnosis of Alzheimer's

Radiotracer	Strength	Limitation
[11C] PIB Pittsburg compound (clinical phase)	High amyloid selectivity and affinity, excellent signal-to-noise feature [47]	Short half-life, the requirement of an on-site cyclotron, expertise in carbon-11 radiochemistry, non-specific white matter retention [1, 48]
[11C]SB-13 (clinical phase)	Good brain uptake and brain clearance [49]	high lipophilicity and high non-specific binding in the brain [50]
[11C] BF227 (clinical phase)	Good brain uptake, specific labeling to amyloid plaques [51]	Lipophilicity [52]
[18F]Florbetapir/[18F]AV-45 (Phase III clinical	The longer half-life of 110 min, high sensitivity, and specificity, fast brain kinetics [53]	Radiotracer burden [54]
[18F]Florbetaben, BAY 94–9172, (AV-1) (Phase III clinical)	Good brain penetration, high affinity for amyloid plaques, rapid metabolism [55]	Background brain radioactivity, lipophilic metabolites [20]
[18F]Flutemetamol 18F-3′-F-PIB, GE-067 (Phase II clinical)	Rapid brain entry, high specificity and sensitivity for the in vivo detection of brain Aβ density [36, 56]	Higher lipophilicity and white matter retention [56]
[18F]FIBT (clinical)	High-contrast Aβ-imaging agent, excellent pharmacokinetics, high specificity and binding affinity [40]	The high degree of unspecific binding
[18F]NAV4694, flutafuranol, [18F]-AZD4694 (Phase III clinical)	More specific gray–white matter demarcation and better pharmacokinetic properties [3, 40]	NA
[18F]BAY 1008472 (Preclinical)	Fast brain uptake and fast elimination [44]	Further validations are awaited
[18F]MK-3328 (Phase I clinical)	Low lipophilicity, high binding affinity to Aβ, low BP to white matter, clinical trials are underway [57]	Further validations are awaited

Brain regions involved the frontal cortex, medial and lateral posterior parietal cortices, precuneus Occipital cortex, lateral, temporal cortices, and striatum

NA not available

[11C]4-N-methylamino-4′-hydroxystilbene, a stilbene derivative, has a high binding affinity to amyloid aggregates in the brain and labeling with carbon 11 to give [11C] SB-13 (4 methylamino-40-hydroxystilbene). Preclinical studies in mice showed excellent brain penetration (5.55 and 9.75% dose/g at 2 min) and rapid brain washout (0.72% dose/g at 60 min) with moderate lipophilicity [31]. In vitro autoradiography studies showed a high specific plaque labeling in brain sections of the transgenic mice model; whereas, it showed no binding in the control sections. It also showed favorable pharmacokinetic properties [32]. Although it showed good brain uptake and brain clearance yet, it was unsuccessful due to its high lipophilicity and non-specific binding in the brain.

FDA approved radiotracers

[18F]Florbetapir scan

To overcome the limitation of the shorter half-life of 11C and on-site cyclotron requirement, [18F]-labeled radiotracers were developed. These are the fluorinated analog of PiB. [18F]Florbetapir ([18F] FBP), is also known as 18F-AV-45, an amyloid PET ligand used for the detection of Aβ plaques. In

2011, it was approved by the FDA for diagnostic use in AD. It is small and moderately lipophilic in nature. In vitro binding studies showed a high affinity for aggregated Aβ proteins, efficiency to cross the blood–brain barrier and get easily washed out of the gray matter that does not contain the plaques. It has a long, pseudo stable equilibrium that allows flexibility in image capture timing. It has an advantage over previously reported [11C]PiB as it has a longer half-life of 110 min, which allows its transportation from the site of production to PET scanner facilities centers.

Preclinical studies were performed in mice and non-human primates (rhesus monkey), which showed excellent brain uptake and rapid kinetics[33]. PET studies in monkey revealed it could cross BBB efficiently and activity in the cortex with a peak value at 7 min. Initially, uptake was good in white matter regions, but the activity has a fast washout rate. 4.4% of the injected dose was reflected at the peak post 20 min of injection in the brain, reflecting rapid entry of 18F-AV-45 in the monkey brain (Fig. 5b). In a healthy monkey brain, it has favorable brain penetration, rapid washout along with low non-specific binding as there were no Aβ plaques shown by small animal PET. Biodistribution studies in mice showed rapid brain uptake and fast washout kinetics. It is very quickly cleared from the blood circulation, with only

10% of the radiotracer remaining after 20 min of injection. It is taken up by the brain of the patients within 30 min of injection and is bio-distributed stably upto 60 min. It showed an excellent binding profile in in vitro autoradiography studies of post mortem AD brain samples for the detection of amyloid plaques in the brain[20].

Currently, there are two more structurally similar ^{18}F-labeled tracers targeting Aβ plaques PET agents, which are under active commercial development. These are BAY 94–9172 (AV-1) and ^{18}F-3′-F-PIB (GE-067) [33]. GE-067 is sponsored by GE healthcare under phase II clinical trial in Europe; whereas, AV-1 is in phase II clinical trials by Schering/Bayer. Human studies are now underway for ^{18}F-AV-45 (AV-45) in phase III clinical trials by Avid Radiopharmaceuticals. [^{18}F]AV-45 biodistribution in humans showed high activity in the liver and gall bladder. There was moderate uptake of activity in the urinary bladder, kidney, and brain; whereas, the accumulation of radioactivity was observed in the intestine. PET studies showed brain uptake of the radiotracer as $5.24 \pm 0.28\%$ID, and $5.04 \pm 0.31\%$ID in healthy controls and AD patients post 10 min of radiotracer injected. Cortical distribution value ratios for [^{18}F] AV-45 were found to be higher in AD patients (1.34–1.6) than healthy controls (1–1.3) as per data of PET brain studies. Biodistribution studies of humans were similar to preclinical data and gave an acceptable variation in the final ED as 5.64 (coefficient of variation). Also, the brain image result showed a fast kinetic, and the highest SUVRcer can be reached within 1 h after injection, which is similar to the time period of the [^{11}C]PIB (50–70 min). [^{18}F] AV-45 was faster than other [^{18}F]-labeled plaque targeting tracers such as [^{18}F]GE067 (85–105 min) [34]. The frontal cortex SUVRcer for [^{18}F]AV-45 was ~30% higher in AD patients than in controls giving the possibility of a radiotracer burden, and this becomes the limitation of this tracer for use (Fig. 6b).

[^{18}F]Florbetaben

Also named as ^{18}F-BAY94-9172 or ^{18}F-AV1/ZK and trans-4-(N-methylamino)-4´-{2-[2-(2-[^{18}F]fluoro-ethoxy)-ethoxy]-ethoxy}-stilbene. It is a ^{18}F-labeled derivative of polyethylene glycol stilbene. In vitro, it binds to neuritic and diffuse Aβ plaques and to cerebral angiopathy. It was found to bind with high affinity (Ki = $6 \cdot 7 \pm 0 \cdot 3$ nM) to the brain homogenate of AD patients. Preclinical studies in mice showed the rapid entry of ^{18}F-BAY94-9172 into the brain with an 8·14% injected dose per gram and washed out in 2 h with 2·14% injected dose per gram. It has rapid metabolism similar to PIB. Also, some of its metabolites are lipophilic, which contributes to the background of brain radioactivity. Ex vivo brain sections of Tg2576 transgenic mice showed localization of this tracer in the Aβ plaques region confirmed by thioflavin T binding. Preclinical studies in several animal

species showed a good profile of [^{18}F]Florbetaben suitable for human studies (Fig. 5c). In healthy patients, initial brain uptake of ^{18}F-BAY94-9172 was higher, and clearance from neocortex was fast as compared to AD patients (Fig. 6c). Cortical ^{18}F-BAY94- 9172 uptake was greater in the frontal and posterior cingulate/precuneus cortex than in the lateral temporal and parietal cortex in AD patients. Histopathological distribution of neuritic plaques matched the binding of ^{18}F-BAY94-9172 to Braak's Aβ deposition categories. The cortical binding of this tracer has provided a robust separation of healthy controls from AD patients. SUVR gives the ratio of binding in the neocortex to the cerebellar gray matter. In AD patients, SUVR was high in the striatum and all cortical regions. Based on clinical criteria, [^{18}F]Florbetaben has 100% sensitivity for the diagnosis of AD by PET with a specificity of 90% [35]. These results suggested the use of [^{18}F]Florbetaben for the detection of Aβ deposition in the early diagnosis and therapeutic monitoring of the disease.

[^{18}F]Flutemetamol

It is also known as [^{18}F] GE067 ([^{18}F] 3′-F-PiB). [^{18}F] GE067 is a structural thioflavin analog of 11C-PIB. [^{18}F] Flutemetamol biodistribution was evaluated in wild-type rats and mice. It revealed similar pharmacokinetics and faster metabolism than [^{11}C] PIB, particularly with white matter. [^{18}F] GEO67 has fast brain uptake in rats, peaked maximum at 5 min with the highest uptake at 5 min in the frontal cortex, and the striatum at 15, 30, and 60 min. PET imaging showed the tracer uptake in the brain. [^{18}F]flutemetamol rapidly entered the brain of rats and excreted via the hepatobiliary pathway. Effective dose estimates were 2.28 and 6.65 μSv/MBqfor [^{11}C]PIB and [^{18}F] flutemetamol, respectively. The specific radioactivity of ^{18}F-flutemetamol (980 ± 430 GBq/μmol at the time of injection) was higher than that of [^{11}C]PIB [36].

In human biodistribution studies, ^{18}F-GE067 was readily taken up in the brain and liver and had rapid excretion through the gastrointestinal system. ^{18}F-GE067 shows predominant hepatobiliary excretion. Human studies showed a total ED of 4.12 ± 0.96 mSv for the PET and 1.5 mSv for the CT parts identical to its structural analog 11C-PIB (estimated ED for ^{11}C-PIB, 4.7 ± 0.8 mSv/MBq). The effective dose of [^{18}F]flutemetamol in humans has been reported to be 33.8 μSv/MBq [37]. Higher lipophilicity and white matter retention limit the sensitivity of this PET tracer (Fig. 6d).

Studies showed the limitations of the FDA approved flutemetamol and florbetaben. When insoluble Aβ levels are low, they have a high level of non-specific white matter retention due to a spill-over effect of radioactivity to adjacent cortical regions from non-specific binding in white matter. Therefore, they should not be used for mapping of Aβ plaque load in prodromal phases and low-density regions

of Alzheimer's [10]. So, the new-generation of Aβ-PET tracers is required, which should have improved signal-to-noise ratio, better pharmacokinetics, and more suitable for the quantification of disease progression and therapeutic monitoring.

Second-generation amyloid PET tracers (Benzofuran, Benzoxazole, and Imidazobenzothiazole derivatives)

[^{11}C]-BF-227

2-(2-[2-dimethylaminothiazol-5-yl]ethenyl)-6- (2-[fluoro] ethoxy)benzoxazole (BF-227), is designed for in vivo detection of dense amyloid deposits using PET. In vivo binding of BF-227 to amyloid plaque deposits was evaluated in mice. In vitro binding assay indicated the high binding affinity of BF-227 for Aβ 1–42 fibrils. Biodistribution study revealed excellent brain uptake and specific labeling of plaques by this tracer in the brain of transgenic mice. This tracer readily penetrated BBB upon the Intravenous administration of BF-227 into normal mice. Clinical dynamic PET images were taken post administration of ^{11}C-BF-227. Using the temporal SUV ratio, healthy controls can be distinguished from AD patients. BF-227 revealed the retention of BF-227 in cerebral cortices of AD patients only. Cortical BF-227 retention in AD patients was distributed to the areas containing depositions of dense Aβ fibrils. BF-227 clearance was slow from the brain due to its lipophilicity. Modification of this compound by adding a hydroxyl group can increase hydrophilicity, which is expected to clear faster than BF-227 and show better signal to noise ratio from the normal brain [38] (Fig. 6e).

[^{18}F]FIBT

Several Imidazo[2,1-b]benzothiazoles (IBTs) were developed and underwent a preclinical trial. Yousefi et al. Group considered 18F-fluorinated [^{18}FIBT] as the best imidazobenzothiazole derivative with favorable in vitro, ex vivo, and preclinical in vivo characteristics. It was further selected for the investigation towards use in humans for the diagnosis of neurodegenerative disorders like Alzheimer's disease (AD) using PET. Preclinical studies in mice showed good in vivo stability and comparable regional brain distribution. High-contrast PET imaging in transgenic mice demonstrated excellent brain penetration and suitable washout (Fig. 5d). It displayed excellent pharmacokinetics, and good initial brain uptake was observed in Balb-c mice. FIBT has high binding affinities to synthetic Aβ aggregates ($K_i = 2$ nM for Aβ1−40 and $K_i = 3$ nM for Aβ1−42) and suitable lipophilicity (log $P = 1.9$) in mice. [^{18}F]FIBT PET images in humans (using 70−90 min static frames) fulfilled the required features

for clinical diagnosis through strong image signal and high image contrast[39, 40] (Fig. 6f). Pharmacokinetics of [^{18}F] FIBT was superior to [^{18}F]florbetaben resulted in better PET ratios (1.68 ± 0.15 versus 1.35 ± 0.06) in transgenic mice. Autoradiography studies of post mortem AD brain confirmed the higher binding affinity of FIBT($K_d = 0.7 \pm 0.2$ nM) than [^{18}F]FIBT ($K_d = 0.7 \pm 0.2$ nM) to Aβ aggregates [39].The ^{18}F-fluorinated imidazo[2,1-b]benzothiazole [^{18}F]FIBT was characterized as a PET tracer by in vitro and ex vivo properties in humans.

[^{18}F]AZD4694/([^{18}F]NAV4694)

2-[2-^{18}F-fluoro-6-(methylamino)-3-pyridinyl]-1-benzofuran-5-ol (18F-NAV4694, formerly known as AZ4694) is an Aβ imaging agent, also known as [^{18}F]Flutafuranol. Its structure and imaging characteristics are similar to ^{11}C-PiB but with the convenience of ^{18}F labeling. ^{18}F-NAV4694 showed high affinity for β-amyloid fibrils in vitro ($K_d = 2.3 \pm 0.3$ nM). Preclinical studies in rats demonstrated a favorable pharmacokinetic profile. It rapidly enters the brain and quickly cleared from the brain of the rat. In aged Tg2576 mice, ex vivo binding showed selective binding to β-amyloid deposits. It has a fast metabolism, and the metabolites were polar [41]. Preclinical profile and certain favorable features of this tracer led its use for PET visualization of cerebral β-amyloid deposits in living human brain. In AD subjects, it selectively labeled β-amyloid deposits in gray matter. PET images showed the binding of [^{18}F]AZD4694 in the cerebral cortex and striatum. Radioactivity was low and homogenously distributed in controls. In contrast, it was higher in the regions containing amyloid plaques in the AD patients [42].^{18}F-NAV4694 has lower non-specific binding to white matter and higher specific cortical binding than other ^{18}F-labeled Aβ radiopharmaceuticals[43] (Fig. 6g).

[^{18}F]BAY 1,008,472

Several fluorinated derivatives were synthesized, which have a nanomolar affinity for Aβ. BAY 1008472 is a fluoropyridyl derivative. In mice, it showed high initial brain uptake (6.45% injected dose per gram at 2 min) and fast brain washout. PET studies were performed in rhesus monkeys for the confirmation of high initial brain uptake of this tracer (SUVR at peak 2.52). PET studies also revealed fast metabolism/elimination of radioactivity from the gray and white matter regions. Autoradiography studies in human brain tissue demonstrated selective binding of BAY 1008472 to Aβ plaques. Ex vivo autoradiography studies were performed in amyloid precursor protein-transgenic mice for the confirmation of in vivo detection of Aβ plaques through BAY 1008472 with good contrast [44]. Considering all the

preclinical parameters, BAY 1008472 can be a good candidate for imaging of amyloid plaques in humans (Fig. 5e).

[^{18}F]MK-3328

Four fluoroazabenzoxazoles were synthesized and evaluated in vitro as amyloid plaque PET tracers. These were AD-278, AD-269, MK-3328, and AD-265. All four compounds displayed high binding affinity in human AD brain cortical homogenates. PET scans in rhesus monkey were done to evaluate the regional distribution and kinetics of all the four tracers. AD-265 was the least potent ligand followed by AD-269 and MK-3328 with slightly more potency and AD-278 as the most potent ligand (IC$_{50}$ = 4 nM).

Nevertheless, AD-278 had moderate binding potential (BP) in the white matter, whereas MK-3328 and AD-269 showed the least BP with the most favorable kinetic profile. All four ligands were moderately lipophilic. In monkey, MK-3328 showed low lipophilicity, high affinity for amyloid plaques, and a favorable combination of low in vivo BP in white matter and cortical gray matter. Lack of binding in the cerebellum of AD patients showed the low levels of amyloid plaque deposits, confirming the specificity of MK-3328 towards the amyloid plaque [45]. It was further investigated in healthy controls and AD subjects until the premature termination of the phase I clinical trial (Fig. 5f).

Chalcone-based PET tracers

FPEG chalcone derivatives

The FPEG (fluoropolyethylene glycol) chalcone derivatives are used as in vivo PET imaging agents to detect Aβ plaques in the brain. Out of various derivatives, one with a dimethylamino group displayed a greater affinity for synthetic Aβ aggregates than the other derivatives. It was labeled with both ^{11}C and ^{18}F. For ^{11}C-labeled FPEG chalcones, biodistribution studies showed sufficient uptake for the imaging of Aβ plaques in the normal mice brain. [^{18}F]-labeled FPEG chalcone also displayed high uptake in and good clearance from the brain. Although very little difference was observed between the ^{11}C and ^{18}F tracers, such as in pharmacokinetics of the tracers. [^{18}F]tracer displayed higher uptake (3.48%ID/g) post-injection of 2 min than ^{11}C-labeled tracer, a level sufficient for imaging. In vitro autoradiographic study in AD patients displayed high levels of radioactivity of [^{18}F] tracer in some specific areas of the brain section[58].

[^{68}Ga] DT(Ch)$_2$

An N,N-dimethylated amine derivative of chalcone labeled with metal radioisotope 68-gallium was evaluated as a PET imaging agent for diagnosis of AD. A DTPA (diethylenetriaminepentaacetic acid) derivatized chalcone system was introduced by Chauhan et al., which attaches to β-amyloid plaques strongly than the tau proteins present in the brain [59]. This chalcone system is developed by conjugation of two chalcone units with DTPA as the chelating system. Bischalcone derivative,5,8-bis(carboxymethyl)-13-(4-((E)-3-(4(dimethylamino)phenyl)acryloyl)phenoxy)-2-(2-(2-(4((E)-3-(4-(dimethylamino)phenyl)acryloyl)phenoxy)ethylamino)-2-oxoethyl)-10-oxo-2,5,8,11-tetraazatridecane-1-carboxylic acid, DT(Ch)$_2$ was synthesized and evaluated in vitro for its binding affinity towards amyloid plaques. The ^{68}Ga-DTPA-conjugated two-chalcone structure showed an 85% radiolabeling yield. The developed ^{68}Ga complex possessed favorable properties such as high binding affinity towards Aβ aggregates, low toxicity, water solubility, high brain uptake, high thermodynamic, and kinetic stabilities required for clinical use. PET images displayed a significant amount of activity in the brain at 2 min p.i. and rapid washout from the healthy brain [60]. Chauhan et al. also reported another chalcone-based homodimeric ligand, (2E,2′E)-1,1′-(((((methylazanediyl)bis(ethane-2,1-diyl))bis(oxy))bis(4,1-phenylene))bis(3-(4(dimethylamino)phenyl)prop-2-en-1-one) [(Chal)$_2$DEA-Me] for imaging of Aβ plaques after labeling with carbon-11[^{11}C] radioisotope. In this, two chalcone moieties possessing the terminal dimethylamino group have been tethered with the help of a linker. Dynamic PET brain imaging in normal Sprague Dawley rats displayed brain uptake kinetics and penetrating the ability of dimeric ligand into BBB. This ligand showed high initial brain uptake and rapid washout required for obtaining high-contrast imaging in the AD brain [61].

PET ligands for detection of tau pathology

Tau aggregates are found in high concentration in temporoparietal cortices; whereas, amyloid-beta aggregates are high in frontal cortex regions[15]. There are six isoforms of tau found in the human brain that arose from alternate mRNA splicing. These six isoforms are classified based on the number of exons (n) and microtubule-binding repeat/domain (R). The six isoforms are [4R 2N], [4R 2N], [4R 0N], [3R 2N], [3R 1N], [3R 0N] [6]. There is an equal ratio of 4R and 3R in a healthy brain and AD as well. This equilibrium gets altered, and there is an accumulation of tau in NDD (Neurodevelopmental disorder) and tauopathy [20]. Tau aggregates are present in white matter, which makes the radiotracer more specific and selective for the brain regions. Tau radiotracer should have low metabolism and low non-tau binding affinity in NS and other brain regions [62]. The tau tracer should recognize and bind to deposits of all isoforms and address 3R and 4R tau deposits. An ideal PET tau tracer should have a strong affinity for PHF and phosphorylated tau aggregates irrespective of it being low in quantity

Fig. 7 Chemical structures of tau targeting PET imaging agents
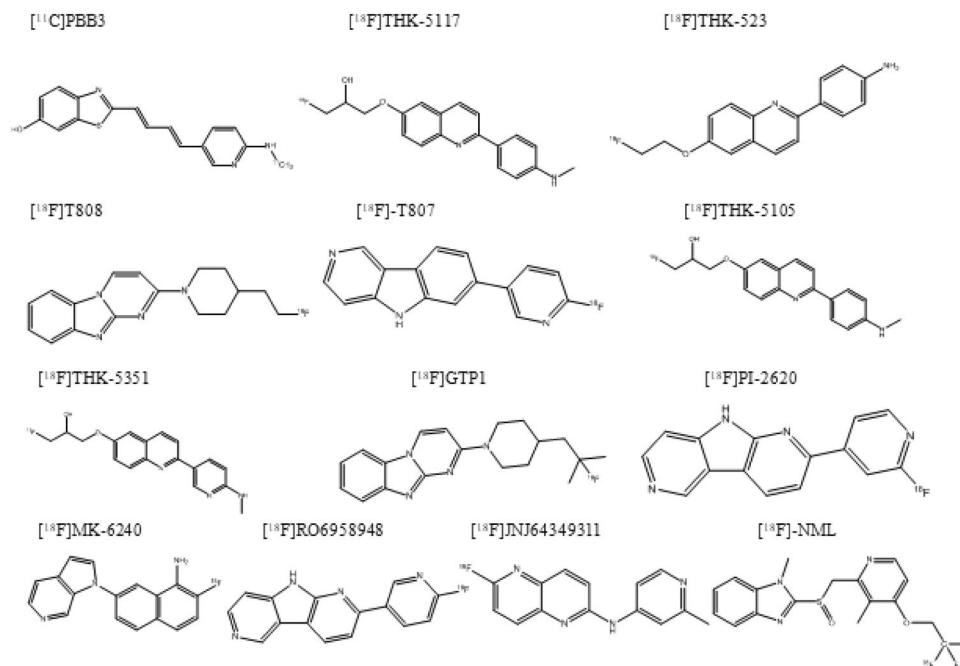
than Aβ aggregates [34, 63, 64]. Figure 7 gives chemical structures of different tau tracers.

## First-generation of PET tau tracers developed so far

[¹¹C]PBB3

2-((1E,3E)-4-(6-(11C-methylamino)pyridin-3-yl)buta-1,3-dienyl)benzo[d]thiazol-6-ol (¹¹C-PBB3) is a clinically useful PET probe developed for in vivo imaging of tau pathology in the human brain. Preclinical studies in mice showed suitable brain uptake (1.92% injected dose/g tissue) and rapid washout from the brain tissue. The biodistribution and metabolite analysis of ¹¹C-PBB3 were evaluated in mice suggesting the radioactivity clearance mainly via the hepatobiliary and intestinal reuptake pathways. [¹¹C]PBB3 was rapidly decomposed to a polar radiometabolite in the plasma of mice.¹¹C-PBB3 easily passed through the blood–brain barrier and is related to its lipophilicity. The effective dose estimate for ¹¹C-PBB3 was 3.28 mSv/MBq [65]. Clinical studies showed the tracer binds specifically to the CA1 and subiculum areas where tau aggregates density is high (Fig. 9a). PBB3 showed a binding affinity for dystrophic neurites as well as neurofibrillary tangles in people suffering from AD. Tracer retention is directly correlated with cognitive decline. [¹¹C]PBB3 binding is associated with gray matter trophy. Like THK5351, the retention of this specific tracer was observed in many parts of the brain like the putamen, midbrain, substantia nigra of patients with different illnesses. There are several drawbacks associated with this tracer, i.e., lower dynamic range, instability

in metabolism, off-target binding in choroid plexus, and basal ganglia. The modified derivatives of PBB3 that are labeled with [¹⁸F], ([¹⁸F]AM-PBB3 and [¹⁸F]-PM-PBB3)) have shown considerable improvement in the drawbacks of PBB3 [66]. [¹⁸F]-PM-PBB3 showed less off-target signals in the basal ganglia than [¹¹C]PBB3 and a greater signal-to-background ratio. Absence of radiometabolites in the brain and no significant off-target binding in the basal ganglia and thalamus were also observed in [¹⁸F]-PM-PBB3.

[¹⁸F]THK5117

[¹⁸F]THK5117 is a phenylquinoline derivative having a binding affinity to tau over Aβ, which is an important property for an ideal tau tracer. In AD brain sections, THK-5117 labeled both 3R and 4R isoforms of tau, suggesting it can recognize specific conformations of tau rather than isoforms. It has fast kinetics in the brain. In AD patients, [¹⁸F]THK-5117 SUVR values for the superior and inferior temporal, orbitofrontal, parietal, and posterior cingulate cortices, as well as for the parahippocampal gyrus, were significantly greater than in HCs. SUVR in the hippocampus was higher for healthy controls. In HC, It showed higher retention in subcortical white matter than the other regions. In AD patients, retention of [¹⁸F]THK-5117 was observed in the temporal lobe known for a region of frequent tau deposits. Non-specific binding in the white matter which reflects its binding to β-sheet structures contained in myelin limits the use of [¹⁸F]THK5117 [67]. [¹⁸F]-THK5117 is more hydrophilic and shows faster pharmacokinetics in mice than [¹⁸F]-THK5105. It showed faster clearance from healthy

Fig. 8 Representative PET images of tau tracers. **a** [^{18}F] THK5117 [68], **b** [^{18}F] THK5351 [68], **c** [^{18}F] S-THK5105 [72] in normal mice, **d** [^{18}F]T807 [80] and **e** [^{18}F]JNJ311 [80] in rhesus monkey, **f** [^{18}F]RO-948 [81] and **g** [^{18}F]MK-6240 [83] in baboon, **h** [^{18}F]PI2620 [88] in rhesus monkey
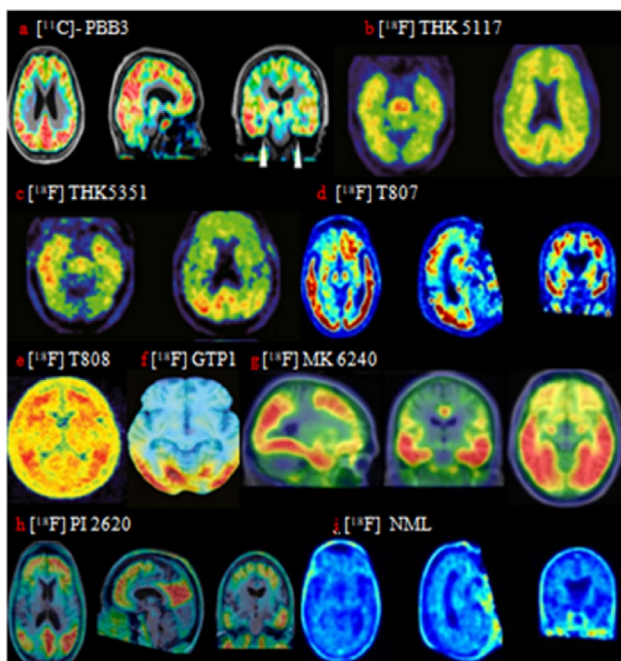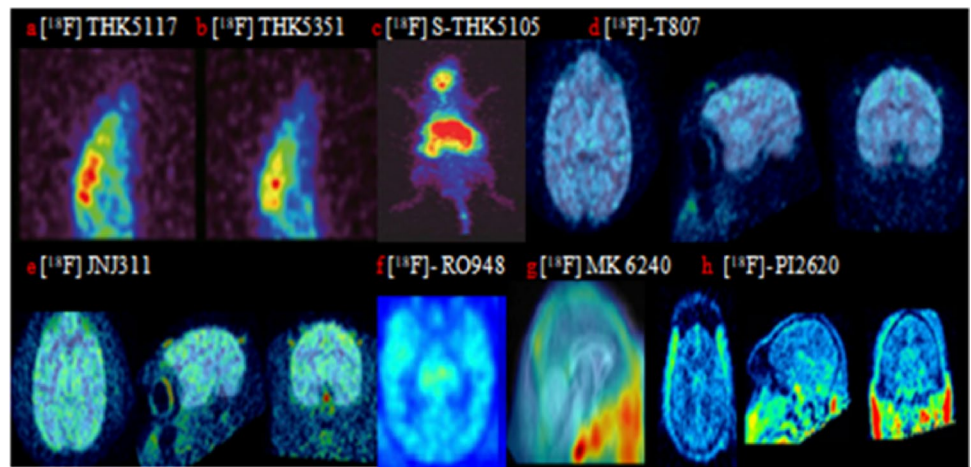
Fig. 9 PET images showing distribution of different tau tracers. **a** [^{11}C]PBB3[62], **b** [^{18}F]THK5117[68], **c** [^{18}F]THK5351 [68], **d** [^{18}F] T807 [90], **e** [^{18}F]T808 [79], **f** [^{18}F]GTP1 [73], **g** [^{18}F]MK-6240 [91], **h** [^{18}F]PI2620 [89], **i** [^{18}F]NML[90] in AD patients

brain tissue in humans and higher signal-to-background ratio as compared to [^{18}F]-THK5105. A clinical trial testing [^{18}F]-THK5117 is currently underway[26] (Figs. 8a, 9b).

[^{18}F]THK5351

To decrease non-specific tracer retention in white matter and to increase the signal-to-background ratio of PET images, a benzene ring of [^{18}F]-THK5117 is replaced with pyridine, and a novel tau PET tracer was developed,

[^{18}F]-THK5351. It is a single S-enantiomer and less lipophilic in nature. Preclinical studies in mice showed rapid pharmacokinetics and more favorable for S-enantiomer (Fig. 8b). It has faster brain clearance than [^{18}F]-THK5117 from the cerebellar cortex. PET studies in mice showed it has rapid brain entry post-injection along with faster washout from the brain. [^{18}F]-THK5351 showed higher contrast and lower subcortical white matter retention as compared to [^{18}F]-THK5117. Preclinical studies revealed a low binding affinity for white matter, high and selective binding ability of this tracer for tau aggregates. Autoradiography studies evaluated the specific binding by the signal-to-background ratio of THK5351, which came out higher than other tracers such as THK5105 and THK5117 [68]. Thus, [^{18}F]-THK5351 is a useful PET tracer for the early diagnosis of neurofibrillary pathology in AD patients [68] (Fig. 9c).

[^{18}F]-THK523

Structural modification of BF-170 gave [^{18}F]-THK-523, a [^{18}F]fluoroethoxy derivative. Ex vivo biodistribution studies of ^{18}F-THK523 in ICR mice displayed brain peak uptake of $2.75 \pm 0.25\%$ ID/g at 2 min post-intravenous injection indicating the adequate lipophilicity of ^{18}F-THK523 to cross the blood–brain barrier. Radiotracer has fast elimination through biliary excretion. [^{18}F]-THK523 radioactivity retention in bone was observed indicative of some degree of defluorination. In vitro saturation binding studies showed its binding to recombinant tau fibrils with high affinity in the low nanomolar range [69]. The autoradiographic analysis indicated the accumulation of [^{18}F]THK-523 in the regions containing a high density of tau protein deposits [70]. Cortical THK523 retention was significantly higher in AD subjects as compared to healthy controls. THK523 showed different brain regional distribution patterns. Unfortunately, clear

visualization of PET scans was not possible due to its high white matter retention, and thus, it was not developed further [71].

$[^{18}F]THK\text{-}5105$

It has a chiral center within a $[^{18}F]$fluoropropanol side chain. The $[^{18}F]$THK5105 contains equal amounts of the (R)-form and (S)-form. Since enantiomers differ in their biological activity, for example, metabolism or binding properties for receptors or plasma proteins, optically pure radioligands may result in different PET or SPECT images compared with their enantiomers. Therefore, it is necessary to characterize each enantiomer for the development of imaging agents with optimal binding properties. The biological evaluation indicated different binding of each enantiomer of $[^{18}F]$THK-5105 in AD brain homogenates and pharmacokinetics in mice. Each enantiomer of $[^{18}F]$THK-5105 revealed different brain kinetics in normal mice. Binding kinetics displayed the affinity of (S)-$[^{18}F]$THK-5105 for tau aggregates are more favorable than those of (R)-$[^{18}F]$THK5105. In normal mice, elimination from the blood and brain is more rapid for (S)-$[^{18}F]$THK-5105 than the (R)-enantiomer [72]. Thus, (S)-enantiomer could be more suitable for a tau imaging agent than the (R)-enantiomer. $[^{18}F]$-THK5105 successfully differentiated AD patients from healthy control subjects as per the clinical findings. PET studies showed lower retention of ^{18}F-THK5105 in the mesial temporal area than in the lateral temporal area in AD patients suggesting higher neurofibrillary tangle density in the entorhinal cortex and hippocampus of Alzheimer's disease brain as compared to the neocortex. Studies showed binding affinity of $[^{18}F]$-THK5105 for tau fibrils ($K_d = 1.45$ nM) was 25-times higher than to amyloid-βfibrils ($K_d = 35.9$ nM). $[^{18}F]$-THK5105 retention in the gray matter was higher; whereas, white matter retention was considerably lower $[^{18}F]$-THK523. In vitro autoradiograms showed a higher signal-to-background ratio of $[^{18}F]$-THK5105 than $[^{18}F]$-THK523 in AD brain sections, which are due to the higher binding affinity of $[^{18}F]$-THK5105 to tau protein fibrils [69, 73]. Also, the peak brain entry of $[^{18}F]$-THK5105 (cerebellar SUV = 4.5) was higher than the other reported radiotracers ($[^{18}F]$-T807, $[^{18}F]$-THK523,$[^{18}F]$-T808 and ^{11}C-PBB3) and similar to the reported SUV value of ^{11}C-PiB. Limitation of $[^{18}F]$-THK5105 is the presence of non-specific tracer retention in the subcortical white matter, brainstem, and thalamus, which reflects the binding of tracer to β-sheet structures present in myelin basic protein [74] (Fig. 8c).

Flortaucipir$[^{18}F]T807$

$[^{18}F]$ flortaucipir is also known as $[^{18}F]$-AV-1451 (T807) and $[^{18}F]$-AV-680 developed by a pharmaceutical company.

It exhibits excellent pharmacokinetic properties, a high binding affinity to PHF, and better selectivity towards tau as compared to amyloid aggregates.$[^{18}F]$-T807 is able to cross BBB and gave good brain PET results. In vivo, PET imaging in mice revealed the rapid penetration and fast washout of $[^{18}F]$T807 in the brain (Fig. 8d). The average peak % injected dose per gram of $[^{18}F]$T807 was 4.16 ± 0.32 at 2 min post-injection and cleared to skeletal muscle levels in about 25 to 30 min. There was some accumulation of the tracer in the bone because of defluorination, which results in the release of $[^{18}F]$fluoride into the blood. Biodistribution in mice exhibited rapid clearance from the brain, with activity values decreasing from 4.43% ID/g at 5 min to 0.62% ID/g at 30 min. Elimination of tracer was through kidney showing maximum tracer concentration of 14.99% ID/g in the kidneys at 5 min, which decreased to 5.52% ID/g at 30 min [75]. The majority of the radiotracer was distributed primarily in three major organs: the bladder, the kidneys, and least to the liver. Autoradiography studies showed the strong binding to native PHF-tau aggregates and weak or no interaction with amyloid plaques in human AD brain sections. In vitro saturation binding studies demonstrated the K_d value in the nanomolar range for the $[^{18}F]$T807 binding to PHF-tau [76]. Initial clinical studies in AD subjects showed the rapid distribution of the tracer, low white matter retention (SUVR $\sim$ 1.0), and high retention in the cortical regions. $[^{18}F]$T807 showed favorable kinetics, rapid delivery into the brain, and clearance from the white matter. It has a low non-specific binding of tracer in white matter and the cortical gray matter of healthy controls. PET scans of the first human study showed the in vivo imaging of PHF-tau in AD subjects showing rapid clearance from plasma and properties suitable for tau quantification with PET (Fig. 9d). Kinetic analysis revealed the separation of cerebellum TAC from the elevated cortical regions starting at 30 min post-injection of AD patients [64, 75]. The binding of Flortaucipir co-localizes with tau deposits only. Clinical PET studies have shown preferential retention of tracer in the region with high tau deposits in AD patients. Like the other tracers, the retention of these tracers in a specific region of the brain is directly correlated with cognitive decline and severity of dementia. Early-onset AD cases have higher flortaucipir uptake than other cases of AD. But high tracer retention is observed in areas where tau pathology is not frequently observed along with off-target binding [77, 78].

$[^{18}F]T808$

$[^{18}F]$-T808 displayed similar selectivity and tau affinity in vitro and in vivo preclinical studies, but it displayed faster pharmacokinetics than $[^{18}F]$-T807 in rodents. Autoradiography studies showed its selectivity of PHF-tau over Aβ plaque was > 27-fold in human cortical brain sections. Also, $[^{18}F]$-T808 has little white matter binding, non-detectable or minimal binding toward

off-target proteins such as MAO or other brain receptors. Preclinical imaging was performed in mice demonstrating suitable brain uptake and washout. [^{18}F]-T808 underwent slow defluorination in rodents as compared to [^{18}F]-T807. [^{18}F]-T808 clinical PET scans showed the favorable distribution and uptake kinetics of this radiotracer with a rapid delivery into the brain and clearance from non-target tissues (Fig. 9e). These findings suggested the possibility of brain imaging as early as 30 min post-injection. There was low tracer retention in white matter and cerebellum. In HC, significantly less radiotracer retention was observed in the cortical gray matter. There was radioactivity in the bone due to [^{18}F]-deflourination which was separated from the cortical brain matter and didn't interfere with the image evaluation even at early time points. The dynamic image analyses, minimal non-specific binding, high targeted cortical radiotracer retention, and favorable kinetic properties of [^{18}F]-T808 across both HC and AD subjects optimize it for a tau-targeting PET imaging agent [79].

Quinolines and benzimidazoles were modified and radiolabeled with [^{18}F] to give rise to [^{18}F]THK-523, [^{18}F]THK5105, [^{18}F]THK-5117/ [^{18}F]THK-5317(17), (S)-[^{18}F]THK-5117 ([^{18}F]THK-5317), [^{11}C]PBB3, [^{18}F]Flortaucipir (AV-1451, [^{18}F]T807), [^{18}F]T808. [^{18}F]THK5105 and [^{18}F]THK5117, which showed improved binding affinity to PHF-tau. The amount of retention of these tracers in the neocortex was correlated to the severity of dementia. The (S) enantiomers of the [^{18}F]THK5117 have better pharmacokinetic properties when compared to the (R) enantiomers. High retention of (S) enantiomers-[^{18}F]THK5317 is a result of mild cognitive impairment and AD dementia. But these, [^{18}F]THK5317 and [^{18}F]THK5117 tracers, have a drawback in binding to the white matter, possibly to the β-sheet structures of myelin proteins.

To overcome these drawbacks, a new radiotracer was developed, namely, [^{18}F]THK5351. This radiotracer had a faster white matter clearance and a higher affinity for tau proteins. However, later this [^{18}F]THK5351 was proved to be less potent because it showed binding in other regions of the brain in people who did not suffer from AD but other diseases that were infrequently related to tau protein accumulation[10].

Second-generation Tau tracers

[^{18}F]GTP1

A deuterated analog of [^{18}F]-T808, [^{18}F]-GTP1(Genentech Tau Probe 1) was designed to improve the radiotracer stability from defluorination. A clinical PET study showed it helps in the differentiation of AD patients from healthy controls as it prevents the accumulation of tracer in the skull [29]. Preclinical imaging studies in mice and rhesus monkeys showed rapid brain uptake and clearance of [^{18}F]-GTP1. Radioactivity was observed in the skull due to the low defluorination of [^{18}F]-GTP1 in both mice and monkeys. Pons and white matter exhibited the lowest uptake level of the tracer. In AD tissues, [^{18}F]-GTP1 exhibited high affinity and selectivity for tau pathology with no measurable binding to β-amyloid plaques or MAO-B or any other protein. [^{18}F]-GTP1 displayed favorable dosimetry and brain kinetics in humans. There was no evidence of defluorination. In vitro, [^{18}F]-GTP1 has higher metabolic stability than [^{18}F]-T808. This suggests that [^{18}F]-GTP1 is unlikely to be metabolized to generate [^{18}F]fluoride in human subjects [73] (Fig. 9f).

[^{18}F]JNJ64349311(JNJ311)

It is a derivative of 1,5-napthyridine showing fast brain clearance and quick metabolism. A preclinical evaluation was done in mice, rats, and rhesus monkeys. A favorable pharmacokinetics profile is an important feature required for the development of PET tracer. This was confirmed by the biodistribution studies performed in mice showing good brain penetration capability of JNJ311. Small animal PET scan was done on both mice and monkeys, which revealed moderate initial brain uptake (SUV as 1.5 at 1 min in Wistar rat and 1.9 at 1 min in rhesus monkey post-injection) and rapid brain washout (Fig. 8e). Plasma radiometabolite analyses showed fast radiotracer metabolism in mice and monkeys. Also, it does not show the presence of polar metabolites in the brain but showed in plasma post-injection of JNJ311. Thus, radiometabolites are not able to cross BBB. Pharmacokinetics (PK) prediction in humans was made based on PK study done in mouse, dog, and rat, indicating fast clearance in humans. No bone uptake was seen post-injection of 60 min and 120 min scan in the mice and monkey, respectively. Based on its high specificity and affinity (K_i value, 8 nM) for aggregated tau over β-amyloid, it is considered as an optimal candidate. Although there are no in vivo human data for this JNJ311 series still based on its in vitro and in vivo preclinical studies, it is considered as a promising candidate for tau imaging by PET in AD [80].

[^{18}F]RO6958948 (RO-948)

After knowing all the drawbacks associated with the tracers initially developed, researchers tried developing new tracers with a better binding affinity, selectivity, and pharmacokinetic property of tau PET tracers. [^{18}F]RO6958948 (RO-948), [^{11}C]RO6931643 (RO-643), and [^{11}C]RO6924963 (RO-963) were high-affinity competitors of 3H-T808, which was a binding site on tau aggregates.

Preclinical studies were performed in baboons revealing pharmacokinetic properties for all three tracers. PET scans showed good brain penetration, rapid washout, and

rapid metabolism pattern post intravenous administration of [^{18}F]-RO6958948, [^{11}C]-RO6931643 and ^{11}C-RO6924963 to baboons. All three tracers showed strong blood to brain clearance having 1.2–2.0 SUVs post-injection of radiotracer and scan initiation. Radioactive uptake in the baboon's brain was distributed homogenously. There was no increased uptake in the white matter regions. For RO-948 and RO-643, radioactivity cleared rapidly from the baboon brain with SUV less than 0.5 at 60 min after injection, whereas radioactivity washout from the brain for RO-963 was slower [81]. RO-948 showed lower regional variations in total distribution volume with higher SUV peak and K_i values. Comparison of three tracers based on in vivo characteristics in non-human primate PET suggested RO-948 is a promising radiotracer in the imaging of tau pathology in AD out of the three. In young controls, [^{18}F]-RO-948 showed the maximum brain penetration and the highest SUV peak at 3.5, followed by ^{11}C-RO-963 at 3.0 and for ^{11}C-RO-643 at 1.5 in the temporal lobe [82]. A regional analysis of SUV ratio and total distribution volume of (RO-643) and (RO-948) discriminated against the AD group from people who were not suffering from AD. (RO-643) was least penetrable to the brain as compared to the other tracers [78]. [^{18}F]-RO-948 displayed good kinetic profile, little retention in YCs, and no brain penetrating radiolabeled metabolites (Fig. 8f). ^{11}C-RO-963 has non-specific binding as it showed retention and slow washout in the young controls. AD subjects showed regional distributions consistent with published post-mortem data on PHF tau; whereas, healthy subjects showed minimal retention. These studies spectacle [^{18}F]-RO-948 as a promising radiotracer for tau imaging.

[^{18}F]-MK-6240

In vitro screening led to the identification of MK-6240, which displayed a high affinity for NFTs ($K_i = 0.36 \pm 0.8$ nM) and weak affinity for amyloid plaque (K_i of 10 mM) in AD brain homogenates. In vitro binding assays showed the poor binding of MK-6240 to amyloid plaque-rich and NFT-poor AD brain homogenates. PET studies were performed in rhesus monkeys to evaluate kinetics and biodistribution of this tracer in the brain. Monkey PET studies showed that it rapidly achieved high levels of brain penetration, followed by rapid clearance (Fig. 8h). Distribution was homogenous, with no increased white matter retention and moderate lipophilicity. Saturation binding studies indicated no displaceable binding of ^{3}H-MK-6240 to non-AD brain donors; whereas, ^{3}H-AV-1451 showed high affinity and displaceable binding in the same pools of brain tissue homogenate. MK6240 showed favorable features for PET tracers such as non-P-gp substrate and good cell permeability, building the potential for good sensitivity for NFTs in human subjects[83, 84]. In vitro autoradiography studies showed higher

contrast of [^{18}F]MK-6240 uptake in AD patients than in age-matched CN individuals across the whole brain cortex, with the highest binding in the PCC, precuneus, inferior parietal, and lateral temporal cortices. In vivo, it displayed favorable kinetics and fast clearance with brain delivery [85]. [^{18}F]-MK6240 DVR values in AD patients were high (DVR > 4), suggesting a combination of high in vivo affinity to tau and low non-displaceable signal. [^{18}F]-MK-6240 was produced on the AllinOne platform yielding high(30 ± 5% non-decay corrected (NDC)) and stable product over time [86]. The kinetics properties of [^{18}F]-MK-6240 were favorable for PET imaging and comparable to the widely used PET radiotracer [^{18}F]-AV-1451 [87] (Fig. 9h).

[^{18}F]-PI-2620

[^{18}F]-PI-2620 displayed a high binding affinity for aggregated tau deposits within the nanomolar range. Preclinical studies showed its binding to both 3-repeat and 4-repeat tau isoforms, which is an important criterion for being a PET tracer. In vivo pharmacokinetic profiling was done in mice and non-human primates (NHP), showing fast brain uptake and complete washout from the mouse brain and having no defluorination (Fig. 8h). The fast clearance demonstrated no off-target binding and gave standardized uptake values (SUVs) of less than 0.3 at 60 min p.i.[88]. Ligand binding assays using (non-demented control) NDC brain tissues revealed an extremely low background binding in brains devoid of pathological misfolded tau. Clinical data obtained in AD and HC subjects displayed a high image quality and excellent signal-to-noise ratio of[^{18}F]-PI-2620 PET for tau imaging in AD subjects (Fig. 9h). Non-invasive quantification using (distribution volume ratios) DVR and SUVR for 30-min imaging windows between 30 and 90 min after injection provides robust and significant discrimination between AD and HC subjects. Also, washout was slower in AD subjects than in HCs in those areas where an accumulation of neurofibrillary tangles can be expected [89].

[^{18}F]N-methyl-lansoprazole

[^{18}F]-NML has high affinity for heparin-induced tau filaments ($K_d = 0.7$ nM) and 11.7-fold selectivity for tau over amyloid. Autoradiography and binding affinity studies confirmed that binding of [^{18}F]-NML to both the 3R/4R tau found in AD patients ($K_d = 8.2$ nM) and 4R tau found in PSP ($K_d = 11.4$ nM). In vivo preclinical imaging studies in healthy rodents, and non-human primates also revealed its high brain uptake and favorable imaging properties and brain pharmacokinetics. The biodistribution studies in male and female Sprague Dawley rats confirmed the brain uptake of the radiotracer. Imaging results in healthy subjects and MCI/AD patients displayed excellent penetration into brain tissue

Clinical and Translational Imaging (2021) 9:153–175

169

Table 2 Tau PET imaging radiopharmaceuticals

Radiotracer	Strength	Limitation
[11C]PBB3 (clinical phase)	Highly selective for tau with good binding affinity having 48 tau/Aβ ratio [10]	Brain penetrating metabolites, instability in metabolism, off-target binding [66]
[18F]THK5117 (clinical phase)	Better kinetics in the brain, more hydrophilic [67, 92]	White matter retention [10]
[18F]-THK5351 (clinical phase I)	Fast pharmacokinetics, high contrast, and low white matter retention, sensitive detection of tau pathology, High affinity of hippocampal homogenates in AD brains, and rapid separation from white matter tissue [68]	off-target binding to monoamine oxidase increased binding in the cortical regions of AD patients [68]
[18F]THK523 (clinical phase)	High affinity and selectivity for tau pathology[92]	White matter retention, failed to detect tau deposits in these non-Alzheimer's disease tauopathies [69]
[18F]THK5105 (clinical phase)	Low white matter retention[74]	non-specific tracer retention in the brainstem, thalamus, and subcortical white matter, which reflects the binding of tracer to b-sheet structures present in myelin basic protein [67]
[18F]T807 (Phase III clinical)	Exhibit good pharmacokinetic properties, high binding affinity to PHF, and better selectivity towards tau (tau/Aβ as 25)[10]	Display higher radioactive background signal after 60 min [64]
[18F]T808 (clinical phase)	Lower non-specific binding, desirable brain kinetics[79]	substantial metabolic instability resulting in apparent defluorination and [18F] fluoride accumulation in bone[73]
[18F] GTP (clinical phase I)	Favorable brain kinetics and improvisation to defluorination[73], clinical trials are underway[93]	NA
[18F] JNJ311 (preclinical)	Fast metabolism [80]	Further validation and clinical studies are awaited
[18F] RO-948 (clinical phase I)	Rapid washout, good kinetic profile, clinical trials are underway[94]	NA
[18F]-MK-6240 (clinical phase)	Homogenous distribution with no increased white matter retention and moderate lipophilicity. High selectivity for tau showing > 27,777 selectivity ratio of tau/Aβ [10, 83] Clinical trials are underway [95]	Low levels of defluorination, test reliability is to be further validated [83]
[18F]-PI-2620 (cinical phase)	Excellent signal-to-noise ratio for tau imaging [89], clinical trials are underway[96]	NA
[18F]-NML (clinical phase)	Good pharmacokinetics, more affinity to tau than amyloid [90]	Failure in the clinical trial [90]

Brain regions involved are the frontal cortex, temporal cortex, parietal cortex, and hippocampus/entorhinal region

NA not available

Springer

with a peak uptake of 5.0–6.0% of the injected dose (i.d.), one-minute post-injection (p.i.), and rapid clearance from brain tissue (Fig. 9i; Table 2). Although this tracer showed good brain uptake, good pharmacokinetics, and appropriate imaging characteristics in healthy controls, it is still not clear to understand the reason for its failure in a clinical trial[90].

In vivo *imaging of neuroinflammation by PET ligands*

Apart from amyloid-beta and tau, neuroinflammation also contributes to the pathophysiology of Alzheimer's disease. Neuroinflammation is a response of innate immunity, which includes astrocytes, microglia, chemokines, and various cytokines [97]. In AD, neuroinflammatory reaction initiates with the activation of microglia, which binds to the surface of soluble and fibrillary Aβ by interacting with surface receptors like TLR4, TLR6, and CD36 along with the production of pro-inflammatory cytokines. Microglia has different roles in AD pathology [98]. In healthy brains, microglia helps in clearing Aβ peptides aggregates by secretion of proteolytic enzymes. In contrast, it releases pro-inflammatory cytokines such as IL-1β and TNF-α in advanced stages of AD and promotes neuronal survival and neuronal cell death. In AD, the accumulation of amyloid-beta oligomers also promotes neuroinflammation by elicitation of proinflammatory cytokines from activation of microglia and interferes with the synthesis of anti-inflammatory cytokines [97, 99].

TSPO is an 18-kDa translocator protein, also known as peripheral benzodiazepine receptor (PBR). It is located on the outer membrane of mitochondria and has a physiological role in cellular respiration, transport of cholesterol, and immunomodulation. It has low expression of TSPO in specific sites of CNS like olfactory bulbs, choroid plexus, endothelial cells, the smooth muscle of the tunica media of intra-parenchymal and extra-parenchymal arteries. Studies showed that microglial activation could be correlated with the radioligand binding of TSPO. Thus, TSPO can detect changes in microglial phenotype and cell morphology associated with neuroinflammation.

[11C]PK11195 was the first TSPO PET tracer used for the detection of neuroinflammation in the brain [100]. [11C]PK11195 PET detected microglial activation associated with amyloid deposition in around 50% of patients with MCI. However, it has several limitations as a shorter half-life of 20 min, poor signal-to-noise ratio, low bioavailability, high plasma binding, non-specific binding due to high lipophilicity [98]. It could not detect little changes in TSPO expression as it has poor BBB penetration and low brain uptake capacity. [11C]PK 11195 did not show binding sensitivity to A147T TSPO, neither in human brain tissue samples nor in clinical PET scans. These limitations led to the development of second-generation ligands for neuroinflammation.
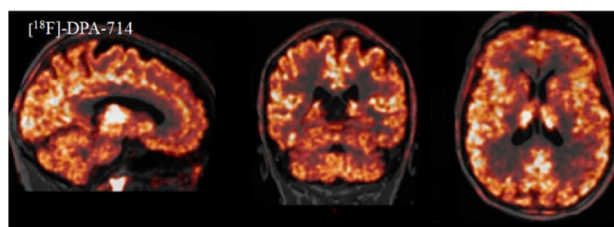

Fig. 10 TSPO PET imaging in Alzheimer's disease using [18F]-DPA-714 tracer in the brain of an AD patient [101]

Second-generation ligands include [11C]-PBR28, [11C]-DPA-713 and [11C]-DAA1106. [11C]-PBR28 has shown 80 fold higher affinity for TSPO and better signal to noise ratio than [11C]-PK11195. [11C]-DPA-713 showed better sensitivity in increased TSPO expression than [11C]-PK11195 [98]. Chauveau et al. have compared the various TSPO radioligands [11C]-DPA-713, [18F]-DPA714, and [11C]-PK11195 in a rat model having acute neuroinflammation. As compared to [11C]-DPA-713 and [11C]-PK11195, [18F]-DPA-714 showed the highest binding and high ratio of ipsilateral to contralateral uptake (Fig. 10). Another ligand, [11C]-DAA1106, showed a tenfold higher affinity in activation of microglia than [11C] PK11195. Due to the shorter half-life of [11C], some more [18F] radioligands were developed. [18F]- FEDAA1106 showed a higher affinity to TSPO than [11C]-PK11195 and [11C]-DAA1106. But [18F]-FEDAA1106 is not able to detect activation of microglia. Further, [18F]-FEMPA was reported as a suitable TSPO PET tracer as it has a high affinity towards TSPO, good pharmacokinetic properties, and high brain penetration [101].

Third-generation ligands include [11C]ER176, a quinazoline analog of PK 11195, with equally high binding at WT and A147T TSPO in membranes prepared from human brain tissue, and improved lipophilicity (log$D$ decreased from 3.97 to 3.55). [11C]ER176 showed higher plasma free fractions and improved PET signal in the monkey brain as compared to PK 11195 [102]. Furthermore, third-generation ligands have an advantage over second-generation ligands as they do not produce radiometabolites that can enter the brain [103]. However, it lacks sensitivity to A147T in human brain-derived membrane preparations. Another ligand, labeled with 18Fistricyclic indole [18F]GE-180 (flutriciclamide). Preclinical models of middle cerebral artery occlusion and AD showed high [18F]GE-180 signals were observed in areas of neuroinflammation in preclinical models of AD with low non-specific binding in the unaffected brain area and low contribution to the brain signal from radiometabolites [104, 105]. Further evaluation of [18F]GE-180 as a neuroinflammation imaging agent in studies with larger sample sizes is required to increase their power to detect genotype differences. The chemical structures of neuroinflammation targeting tracers are drawn in Fig. 11.

Fig. 11 Chemical structures of neuroinflammation targeting PET tracers
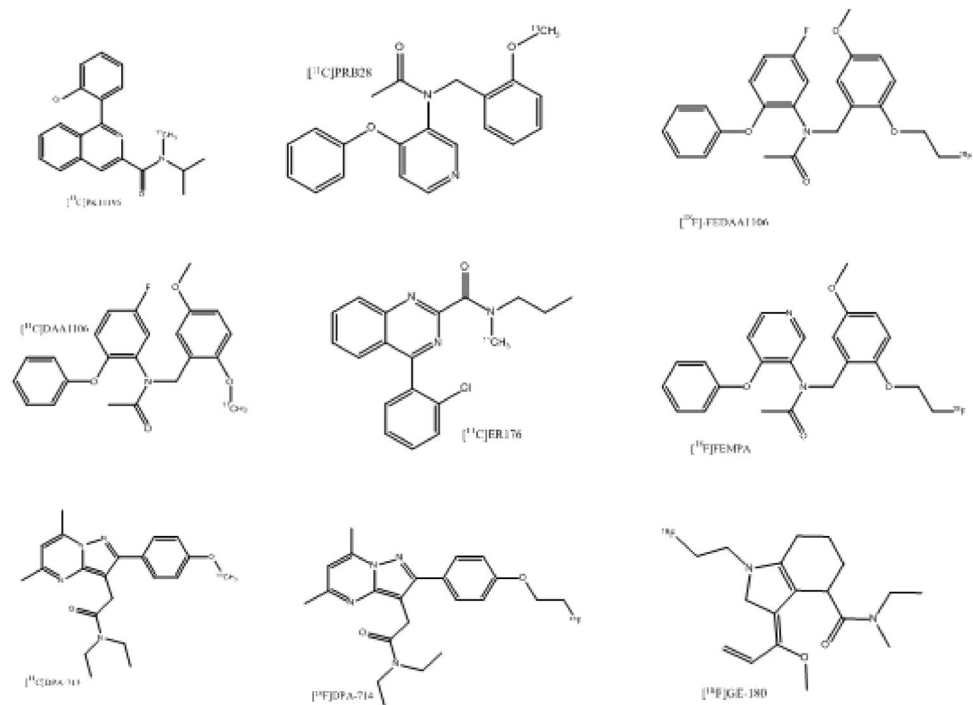
Other targets

Apart from TSPO, there are several other PET targets for early detection of neuroinflammation in AD. These are Cannabinoid receptor type 2, COX1 or COX2, P2X$_7$ receptor, monoamine oxidase.

Cannabinoid receptor type 2 (CB2) is present on presynaptic terminals involved in releasing presynaptic neurotransmitters. It has low expression in a healthy brain; whereas, during inflammation, activated microglia upregulates CB2 expression. In the brain, it has a high density of its receptors, making it a potential target for the detection of neuroinflammation at the early stage of the disease. For PET imaging, the CB2 receptor was modified to 8-Tetrahydrocannabinol (Δ8-THC) labeled with [18]F. However, this radioligand showed low uptake and wide distribution in the brain when injected [101, 106]. Another specific radioligand for CB2 PET was ^{11}C-NE40, which is lipophilic. ^{11}C-NE40 showed favorable features for neuroimaging, and it was used for biodistribution studies in healthy people for uptake and washout verification [107].

P2X7 receptor is an ATP-gated purinoreceptor involved in microglia and astrocytes activation. It serves as a potential biomarker of neuroinflammation. Activation of the P2X7 receptor produces pro-inflammatory cytokines in the brain. Several PET tracers for P2X7 have been reported. Out of those, ^{11}C-GSK1482160, ^{11}C-SMW139, and ^{18}F-JNJ-64413739 showed better results. ^{11}C-GSK1482160 was used to estimate radiation dose and biodistribution studies in a healthy person.

[11]C-SMW139 was administered in 2019 for the first PET/MRI study. Labeled with ^{18}F, ^{18}F-JNJ-64413739 has the advantage of long half-life over others, making it a better PET radiotracer. It is still under evaluation for preclinical studies in the models of neuroinflammation. Current studies showed its potential for PET tracer in the future for neuroinflammation [108].

Cyclooxygenase-2 is involved in cellular responses associated with neuroinflammation. In Alzheimer's, there is an upregulation of the COX2 gene. Celecoxib is a highly selective COX2 inhibitor, FDA approved drug used to develop PET ligand labeled with [11]C. ^{11}C-celecoxib can cross BBB, making it a successful PET tracer [109].

Macrophage colony-stimulating factor 1 receptor (CSF1R) is also known as CD-115 expressed by microglia. CSF-1R plays an important role in the development, survival, maintenance of microglia and neuroinflammation. Inhibition of CSF-1R is one way of treatment of neuroinflammation disorders. Studies show a high expression of CSF-1R in microglia around the amyloid-beta depositions. ^{11}C-CPPC is a PET radiotracer developed for imaging of CSF-1R. This PET ligand is still in the preclinical phases of animal experiments[110].

Monoamine oxidase (MAO) is involved in the regulation of neurotransmitter amines concentration. MAO is a flavin-containing enzyme, with two isoforms, MAO-A and MAO-B, present on outer mitochondria. There is an upregulation of MAO-B in reactive astrocytes during inflammation. MAO-B expressing astrocytes is colocalized with amyloid plaques showing the association of MAO-B in AD.

[^{11}C]DED was used as a radiotracer for MAO-B imaging. Reports suggested MAO-B PET imaging can be used as a measure of astrocytosis in the early onset of disease. After years, carbon-11([^{11}C]-L-deprenylD2) and fluorine-18 ([^{18}F]-THK5351) were developed as radiotracers for MAO-B imaging [111, 112].

Conclusion and future perspective in designing PET tracers for AD

The present review is focused on comprehensive radiotracers developed so far with their strength and limitations for the diagnosis of AD by PET. The aim of performing imaging scans by PET in AD is to non-invasively aid in the diagnosis and provide objective confirmatory evidence of the cause of the neurocognitive disorder. Thus, accurate interpretation can provide a better therapeutic model and management of Alzheimer's disease. Several PET tracers have been developed for the early diagnosis of Alzheimer's, but still, there are some limitations associated with each tracer. There are only three FDA approved PET tracers. Imaging of tau by PET is very challenging in the human brain. Since amyloid-beta aggregates and tau aggregates share structural similarity, it becomes challenging to trace tau aggregates. However, there is a difference in concentration of amyloid aggregates, which is almost 5–20 times higher than tau aggregates, which marks a significant difference in the detection of tau by a radiotracer. Clinical investigation of tau pathology by tau tracers are there in the clinical studies but still pose challenges in selectively imaging tau aggregates.

Positron emission tomography has been very useful in visualizing neuroinflammation in vivo. It helped in elucidating the complex role of the inflammatory process in neurodegenerative diseases by detecting, quantifying, and specifying the topology of inflammation reaction occurring in the brain. PET imaging helps in tracking neuroinflammation for early delivery of therapeutics by tracking the disease progression and response to a novel therapeutic in the clinical trial. PET radioligands targeting TSPO has faced problems due to the presence of a single nucleotide polymorphism producing A147T TSPO at which every disclosed second-generation TSPO PET ligand loses affinity. Although the third-generation ligands have given less discriminating imaging, the development of ligands requires more knowledge of discrimination in WT TSPO and A147T TSPO structure. This can be accomplished by understanding TSPO binding discrimination by structure–affinity relationships through high-throughput screening of ligand binding.

Several factors are responsible for the failure of pharmaceuticals, such as lack of efficacy, poor drug metabolism, toxicity, poor pharmacokinetic profile, and high lipophilicity [100]. PET molecular imaging helps in providing a quantitative measurement for the acceleration of drug development for therapeutics. PET imaging saves both time and money in the selection of targets, dosage, confirmation of mechanisms, and evaluation of drugs in their development. It, thus, helps in better management of Alzheimer's disease pathology. Future works require new imaging radioligands with improved automated quantification and specificity of amyloid imaging, newer techniques for prognostication of at-risk older adults for the possibility of developing Alzheimer's disease.

Compliance with ethical standards

Conflict of interest The authors declare that they have no conflict of interest.

Ethics approval This manuscript does not involve any study on animals or humans.

Consent for publication The manuscript has been seen and approved by all authors for submission.

References

1. Vlassenko AG, Benzinger TLS, Morris JC (2012) PET amyloid-beta imaging in preclinical Alzheimer's disease. Biochim Biophys Acta 1822:370–379. https://doi.org/10.1016/j.bbadis.2011.11.005
2. Birch AM, Katsouri L, Sastre M (2014) Modulation of inflammation in transgenic models of Alzheimer's disease. J Neuro Inflamm 11:1–13
3. Zhang XY, Yang ZL, Lu GM et al (2017) PET/MR imaging: new frontier in Alzheimer's disease and other dementias. Front Mol NeuroSci 10:1–12
4. García-Ayllón MS, Small DH, Avila J et al (2011) Revisiting the role of acetylcholinesterase in Alzheimers disease: cross-talk with β-tau and p-amyloid. Front Mol Neurosci 4:1–9
5. Matsuda H, Shigemoto Y, Sato N (2019) Neuroimaging of Alzheimer's disease: focus on amyloid and tau PET. Jpn J Radiol 37:735–749. https://doi.org/10.1007/s11604-019-00867-7
6. Ariza M, Kolb HC, Moechars D et al (2015) Tau positron emission tomography (PET) imaging: past, present, and future. J Med Chem 58:4365–4382

7. Hane FT, Robinson M, Lee BY et al (2017) Recent progress in Alzheimer's disease research, part 3: diagnosis and treatment. J Alzheimer's Dis 57:645–665

8. Valentina G, Silvia M, Marco P (2016) Dual-phase amyloid PET: hitting two birds with one stone. Eur J Nucl Med Mol Imaging 43:1300–1303. https://doi.org/10.1007/s00259-016-3393-6

9. Son SH, Kang K, Ko PW et al (2020) Early-phase 18F-florbetaben PET as an alternative modality for 18F-FDG PET. Clin Nucl Med 45:E8–E14

10. Landscape F and Parkinson's disease diagnosis, the current 2020. https://doi.org/10.3390/molecules25040977

11. Owen DRJ, Gunn RN, Rabiner EA et al (2011) Mixed-affinity binding in humans with 18-kDa translocator protein ligands. J Nucl Med 52:24–32

12. Werry EL, Bright FM, Piguet O et al (2019) Recent developments in TSPO PET imaging as a biomarker of neuroinflammation in neurodegenerative disorders. Int J Mol Sci 20:1–21

13. Velikyan I (2014) Prospective of 68Ga-Radiopharmaceutical development. Theranostics 4:47–80

14. Nunes-Tavares N, Santos LE, Stutz B et al (2012) Inhibition of choline acetyltransferase as a mechanism for cholinergic dysfunction induced by amyloid-β peptide oligomers. J Biol Chem 287:19377–19385

15. Carvajal FJ, Inestrosa NC (2011) Interactions of AChE with A? aggregates in Alzheimer's brain: therapeutic relevance of IDN 5706. Front Mol Neurosci 4:1–10

16. Majdi A, Sadigh-Eteghad S, Rahigh Aghsan S, et al (2020) Amyloid-β, tau, and the cholinergic system in Alzheimer's disease: seeking direction in a tangle of clues. Rev Neurosci 31:391–413. https://www.degruyter.com/view/journals/revneuro/31/4/article-p391.xml

17. Mier W, Mier D (2015) Advantages in functional imaging of the brain. Front Hum Neurosci 9:1–6

18. James OG, Doraiswamy PM, Borges-Neto S (2015) PET imaging of tau pathology in Alzheimer's disease and tauopathies. Front Neurol 6:1–4

19. Feng H, Wang X, Chen J et al (2019) Nuclear imaging of glucose metabolism: beyond 18 F-FDG. Contrast Med Mol Imaging 7:1–12

20. Suppiah S, Didier MA, Vinjamuri S (2019) The who, when, why, and how of PET amyloid imaging in management of Alzheimer's disease-review of literature and interesting images. Diagnostics 9:25

21. Nordberg A, Rinne JO, Kadir A et al (2010) The use of PET in Alzheimer disease. Nat Rev Neurol 6:78–87. https://doi.org/10.1038/nrneurol.2009.217

22. Dubois B, Feldman HH, Jacova C et al (2014) Advancing research diagnostic criteria for Alzheimer's disease: the IWG-2 criteria. Lancet Neurol 13:614–629

23. Mosconi L, Berti, V, Glodzik L, Pupi A, De Santi S, de Leon M (2010) Pre-clinical detection of Alzheimer's disease using FDG-PET, with or without amyloid imaging. 20–(3):843–854. https://doi.org/10.3233/JAD-2010-091504

24. Shin J, Kepe V, Barrio JR et al (2011) The merits of FDDNP-PET imaging in Alzheimers disease. J Alzheimer's Dis 26:135–145

25. Leuzy A, Chiotis K, Lemoine L et al (2019) Tau PET imaging in neurodegenerative tauopathies—still a challenge. Mol Psychiatry 24:1112–1134

26. Okamura N, Furumoto S, Harada R et al (2013) Novel 18F-labeled arylquinoline derivatives for noninvasive imaging of Tau pathology in Alzheimer disease. J Nucl Med 54:1420–1427

27. Tolboom N, Yaqub M, Van Der Flier WM et al (2009) Detection of Alzheimer pathology in vivo using both11C-PIB and18F-FDDNP PET. J Nucl Med 50:191–197

28. Mathis CA, Wang Y, Holt DP et al (2003) Synthesis and evaluation of 11C-labeled 6-substituted 2-arylbenzothiazoles as amyloid imaging agents. J Med Chem 46:2740–2754

29. Klunk WE, Engler H, Nordberg A et al (2004) Imaging brain amyloid in Alzheimer's disease with pittsburgh compound-B. Ann Neurol 55:306–319

30. Manuscript AEK and CAM (2009) Departments of Psychiatry and Neurology, University of Pittsburgh School of Medicine P, Pennsylvania PU et al. 2012. Development of positron emission tomography β-amyloid.pdf., Psychiatry Interpers Biol Process, vol 21, pp 683–687. https://doi.org/10.1053/j.semnuclmed.2012.07.001

31. Ono M, Wilson A, Nobrega J et al (2003) 11C-labeled stilbene derivatives as Aβ-aggregate-specific PET imaging agents for Alzheimer's disease. Nucl Med Biol 30:565–571

32. Zhang W, Oya S, Kung MP et al (2005) F-18 stilbenes as PET imaging agents for detecting β-amyloid plaques in the brain. J Med Chem 48:5980–5988

33. Choi SR, Golding G, Zhuang Z et al (2009) Preclinical properties of 18F-AV-45: a PET agent for Aβ plaques in the brain. J Nucl Med 50:1887–1894

34. Goedert M, Spillantini MG (2011) Pathogenesis of the tauopathies. J Mol Neurosci 45:425–431

35. Rowe CC, Ackerman U, Browne W et al (2008) Imaging of amyloid β in Alzheimer's disease with 18F-BAY94–9172, a novel PET tracer: proof of mechanism. Lancet Neurol 7:129–135

36. Snellman A, Rokka J, Lopez-Picon FR et al (2012) Pharmacokinetics of [18F]flutemetamol in wild-type rodents and its binding to beta amyloid deposits in a mouse model of Alzheimer's disease. Eur J Nucl Med Mol Imaging 39:1784–1795

37. Koole M, Lewis DM, Buckley C et al (2009) Whole-body biodistribution and radiation dosimetry of 18F-GE067: a radioligand for in vivo brain amyloid imaging. J Nucl Med 50:818–822

38. Kudo Y, Okamura N, Furumoto S et al (2007) 2-(2-[2-Dimethylaminothiazol-5-yl]ethenyl)-6-(2-[fluoro]ethoxy)benzoxazole: a novel PET agent for in vivo detection of dense amyloid plaques in Alzheimer's disease patients. J Nucl Med 48:553–561

39. Yousefi BH, von Reutern B, Scherübl D et al (2015) FIBT versus florbetaben and PiB: a preclinical comparison study with amyloid-PET in transgenic mice. EJNMMI Res 5:20

40. Hooshyar Yousefi B, Manook A, Grimmer T et al (2015) Characterization and first human investigation of FIBT, a novel fluorinated aβ plaque neuroimaging pet radioligand. ACS Chem Neurosci 6:428–437

41. Juréus A, Swahn BM, Sandell J et al (2010) Characterization of AZD4694, a novel fluorinated Aβ plaque neuroimaging PET radioligand. J Neurochem 114:784–794

42. Cselényi Z, Jönhagen ME, Forsberg A et al (2012) Clinical validation of 18F-AZD4694, an amyloid-β-specific PET radioligand. J Nucl Med 53:415–424

43. Rowe CC, Jones G, Dore V et al (2016) Standardized Expression of 18F-NAV4694 and 11C-PiB b-amyloid PET results with the centiloid scale. J Nucl Med 57:1233–1237

44. Brockschnieder D, Schmitt-Willich H, Heinrich T et al (2012) Preclinical characterization of a novel class of 18F-labeled PET tracers for amyloid-β. J Nucl Med 53:1794–1801

45. Hostetler ED, Sanabria-Bohórquez S, Fan H et al (2011) [18F]Fluoroazabenzoxazoles as potential amyloid plaque PET tracers: synthesis and in vivo evaluation in rhesus monkey. Nucl Med Biol 38:1193–1203. https://doi.org/10.1016/j.nucmedbio.2011.04.004

46. Kung HF, Choi SR, Qu W et al (2010) 18F stilbenes and styrylpyridines for PET imaging of Aβ plaques in Alzheimer's disease: a miniperspective. J Med Chem 53:933

47. Klunk WE, Mathis CA (2008) The future of amyloid-beta imaging: a tale of radionuclides and tracer proliferation. Curr Opin Neurol 21:683–687

48. Schilling LP, Zimmer ER, Shin M et al (2016) Imaging Alzheimer's disease pathophysiology with PET. Dement Neuropsychol 10:79–90

49. Hong MC, Kim YK, Choi JY et al (2010) Synthesis and evaluation of stilbene derivatives as a potential imaging agent of amyloid plaques. Bioorg Med Chem 18:7724–7730. https://doi.org/10.1016/j.bmc.2010.06.044

50. Henriksen G, Yousefi BH, Drzezga A et al (2008) Development and evaluation of compounds for imaging of β-amyloid plaque by means of positron emission tomography. Eur J Nucl Med Mol Imaging 35:S75–S81

51. Svedberg MM, Rahman O, Hall H (2019) Preclinical studies of potential amyloid binding PET/SPECT ligands in Alzheimer's disease. Nucl Med Biol 39:484–501. https://doi.org/10.1016/j.nucmedbio.2011.10.007

52. Arakawa Y, Nai Y, Shidahara M et al (2017) PreDiction of the clinical SUV ratio in amyloid PET imaging using a biomathematic modeling approach toward the efficient development of a raDioligand. J Nucl Med 58:1285–1292

53. Lin KJ, Hsu WC, Hsiao IT et al (2010) Whole-body biodistribution and brain PET imaging with [18F]AV-45, a novel amyloid imaging agent—a pilot study. Nucl Med Biol 37:497–508. https://doi.org/10.1016/j.nucmedbio.2010.02.003

54. Landau SM, Breault C, Joshi AD et al (2013) Amyloid-β imaging with Pittsburgh compound B and florbetapir: comparing radiotracers and quantification methods. J Nucl Med 54:70–77

55. Sabri O, Sabbagh MN, Seibyl J et al (2015) Florbetaben PET imaging to detect amyloid beta plaques in Alzheimer's disease: Phase 3 study. Alzheimer's Dement 11:964–974

56. Vandenberghe R, Van Laere K, Ivanoiu A et al (2010) 18F-flutemetamol amyloid imaging in Alzheimer disease and mild cognitive impairment a phase 2 trial. Ann Neurol 68:319–329

57. Description S (2011) [18F]MK-3328 as a possible novel positron emission tomography (PET) tracer for the detection of brain amyloid plaques (MK-3328–002). Clin Trials [Internet] 1–8. https://clinicaltrials.gov/ct2/show/NCT01385033

58. Ono M, Watanabe R, Kawashima H et al (2009) Fluoro-pegylated chalcones as positron emission tomography probes for in vivo imaging of β-amyloid plaques in Alzheimer's disease. J Med Chem 52:6394–6401

59. Barrios-lopez B, Airaksinen A, Bergström K (2015) Gallium-68 radio tracers for Alzheimer's plaque i maging. J Diagn Imaging Therapy 2:50–64

60. Chauhan K, Datta A, Adhikari A et al (2014) 68Ga based probe for Alzheimer's disease: Synthesis and preclinical evaluation of homodimeric chalcone in β-amyloid imaging. Org Biomol Chem 12:7328–7337

61. Chauhan K, Tiwari AK, Chadha N et al (2018) Chalcone based homodimeric PET agent, 11 C-(Chal) 2 DEA-Me, for beta amyloid imaging: synthesis and bioevaluation. Mol Pharm 15:1515–1525

62. Shah M, Catafau AM (2014) Molecular imaging insights into neurodegeneration: focus on tau PET radiotracers. J Nucl Med 55:871–874

63. Villemagne VL, Furumoto S, Fodero-Tavoletti MT et al (2014) In vivo evaluation of a novel tau imaging tracer for Alzheimer's disease. Eur J Nucl Med Mol Imaging 41:816–826

64. Chien DT, Bahri S, Szardenings AK et al (2013) Early clinical PET imaging results with the novel PHF-tau radioligand [F-18]-T807. J Alzheimer's Dis 34:457–468

65. Hashimoto H, Kawamura K, Igarashi N et al (2014) Radiosynthesis, photoisomerization, biodistribution, and metabolite analysis of 11C-PBB3 as a clinically useful PET probe for imaging of tau pathology. J Nucl Med 55:1532–1538

66. Kimura Y, Ichise M, Ito H et al (2015) PET quantification of tau pathology in human brain with 11C-PBB3. J Nucl Med 56:1359–1365

67. Harada R, Okamura N, Furumoto S et al (2015) [18F]THK-5117 PET for assessing neurofibrillary pathology in Alzheimer's disease. Eur J Nucl Med Mol Imaging 42:1052–1061

68. Harada R, Okamura N, Furumoto S et al (2016) 18F-THK5351: A novel PET radiotracer for imaging neurofibrillary pathology in Alzheimer disease. J Nucl Med 57:208–214

69. Fodero-Tavoletti MT, Okamura N, Furumoto S et al (2011) 18F-THK523: A novel in vivo tau imaging ligand for Alzheimer's disease. Brain 134:1089–1100

70. Harada R, Okamura N, Furumoto S et al (2013) Comparison of the binding characteristics of [18F]THK-523 and other amyloid imaging tracers to Alzheimer's disease pathology. Eur J Nucl Med Mol Imaging 40:125–132

71. Fodero-Tavoletti MT, Furumoto S, Taylor L et al (2014) Assessing THK523 selectivity for tau deposits in Alzheimer's disease and non-Alzheimer's disease tauopathies. Alzheimer's Res Ther 6:1–10

72. Tago T, Furumoto S, Okamura N et al (2016) Preclinical evaluation of [18F]THK-5105 enantiomers: effects of chirality on its effectiveness as a tau imaging radiotracer. Mol Imaging Biol 18:258–266

73. Sanabria Bohórquez S, Marik J, Ogasawara A et al (2019) [18F]GTP1 (Genentech Tau Probe 1), a radioligand for detecting neurofibrillary tangle tau pathology in Alzheimer's disease. Eur J Nucl Med Mol Imaging 46:2077–2089

74. Okamura N, Furumoto S, Fodero-Tavoletti MT et al (2014) Non-invasive assessment of Alzheimer's disease neurofibrillary pathology using 18F-THK5105 PET. Brain 137:1762–1771

75. Wooten DW, Guehl NJ, Verwer EE et al (2017) Pharmacokinetic evaluation of the tau PET radiotracer 18F–T807 (18F-AV-1451) in human subjects. J Nucl Med 58:484–491

76. Xia CF, Arteaga J, Chen G et al (2013) [18F]T807, a novel tau positron emission tomography imaging agent for Alzheimer's disease. Alzheimer's Dement 9:666–676. https://doi.org/10.1016/j.jalz.2012.11.008

77. Okamura N, Harada R, Ishiki A et al (2018) The development and validation of tau PET tracers: current status and future directions. Clin Transl Imaging 6:305–316. https://doi.org/10.1007/s40336-018-0290-y

78. Lois C, Gonzalez I, Johnson KA et al (2019) PET imaging of tau protein targets: a methodology perspective. Brain Imaging Behav 13:333–344. https://doi.org/10.1007/s11682-018-9847-7

79. Chien DT, Szardenings AK, Bahri S et al (2014) Early clinical PET imaging results with the novel PHF-tau radioligand [F18]-T808. J Alzheimer's Dis 38:171–184

80. Declercq L, Rombouts F, Koole M et al (2017) Preclinical evaluation of 18F-JNJ64349311, a novel PET tracer for tau imaging. J Nucl Med 58:975–981

81. Honer M, Gobbi L, Knust H et al (2018) Preclinical evaluation of 18F-RO6958948, 11C-RO6931643, and 11C-RO6924963 as novel PET radiotracers for imaging tau aggregates in Alzheimer disease. J Nucl Med 59:675–681

82. Wong DF, Comley RA, Kuwabara H et al (2018) Characterization of 3 novel tau radiopharmaceuticals,11C-RO-963,11C-RO-643,and18F-RO-948, in healthy controls and in Alzheimer subjects. J Nucl Med 59:1869–1876

83. Hostetler ED, Walji AM, Zeng Z et al (2016) Preclinical characterization of 18F-MK-6240, a promising PET tracer for in vivo quantification of human neurofibrillary tangles. J Nucl Med 57:1599–1606

84. Aguero C, Dhaynaut M, Normandin MD et al (2019) Autoradiography validation of novel tau PET tracer [F-18]-MK-6240 on human postmortem brain tissue. Acta Neuropathol Commun. 2019(7):37

85. Pascoal TA, Shin M, Kang MS et al (2018) In vivo quantification of neurofibrillary tangles with [18F]MK-6240. Alzheimer's Res Ther 10:1–14

86. Vriamont C, Otabashi M, Warnier C (2020) High yield production of [F] MK-6240 on the AllinOne synthesizer, a promising PET Tracer for the quantification of human neurofibrillary tangles in Alzheimer disease. J Nucl Med 61:1–2

87. Emadwiandr (2013) In vivo characterization and quantification of neurofibrillary tau PET radioligand ^{18}F-MK-6240 in humans from Alzheimer's disease dementia to young controls. J Chem Inf Model 53:1689–1699. http://file:///E:/preclinical studies/79. 18F-MK-6240 characterization in humans.pdfhttp://file:///E:/preclinical studies/79. 18F-MK-6240 characterization in humans.pdf. https://doi.org/10.2967/jnumed.118.209650

88. Kroth H, Oden F, Molette J et al (2019) Discovery and preclinical characterization of [^{18}F]PI-2620, a next-generation tau PET tracer for the assessment of tau pathology in Alzheimer's disease and other tauopathies. Eur J Nucl Med Mol Imaging 46:2178–2189

89. Mueller A, Bullich S, Barret O et al (2020) Tau PET imaging with 18F-PI-2620 in patients with Alzheimer disease and healthy controls: a first-in-humans study. J Nucl Med 61:911–919

90. Kramer V, Brooks AF, Haeger A et al (2020) Evaluation of [18F]-N-methyl lansoprazole as a tau PET imaging agent in first-in-human studies. ACS Chem Neurosci 11:427–435

91. Betthauser TJ, Cody KA, Zammit MD et al (2019) In vivo characterization and quantification of neurofibrillary tau PET radioligand 18F-MK-6240 in humans from Alzheimer disease dementia to young controls. J Nucl Med 60:93–99

92. Murugan NA, Nordberg A, Ågren H (2018) Different positron emission tomography tau tracers bind to multiple binding sites on the tau fibril: insight from computational modeling. ACS Chem Neurosci 9:1757–1767

93. Genentech (2016) Longitudinal evaluation of [^{18}F]MNI-798 as a PET radioligand for imaging tau in the brain of patients with Alzheimer's disease compared to healthy volunteers. Clin Trials. gov [Internet]. 1:1–8. https://clinicaltrials.gov/ct2/show/NCT02640092

94. Summary T (2020) Evaluation of [18F] RO6958948 as tracer for positron emission tomography (PET) imaging of tau burden in Alzheimer's disease participants 1–8. https://clinicaltrials.gov/ct2/show/results/NCT02792179

95. Description S (2020) [18F] MK-6240 positron emission tomography (PET) tracer first-in-human validation study (MK-6240–001) 1–10. https://clinicaltrials.gov/ct2/show/NCT02562989

96. Kim JS (2020) Evaluation of [^{18}F]PI-2620 as a potential positron emission computed tomography radioligand for imaging tau protein in the brain. https://clinicaltrials.gov/ct2/show/NCT03510572

97. Hampel H, Caraci F, Cuello AC et al (2020) A path toward precision medicine for neuroinflammatory mechanisms in Alzheimer's disease. Front Immunol. https://doi.org/10.3389/fimmu.2020.00456

98. Calsolaro V, Edison P (2016) Neuroinflammation in Alzheimer's disease: Current evidence and future directions. Alzheimer's Dement 12:719–732. https://doi.org/10.1016/j.jalz.2016.02.010

99. Cavaliere C, Tramontano L, Fiorenza D et al (2020) Gliosis and neurodegenerative diseases: the role of PET and MR imaging. Front Cell Neurosci 14:1–13

100. Liu CH, Sastre A, Conroy R et al (2014) NIH workshop on clinical translation of molecular imaging probes and technology—meeting report. Mol Imaging Biol 16:595–604

101. Lagarde J, Sarazin M, Bottlaender M (2018) In vivo PET imaging of neuroinflammation in Alzheimer's disease. J Neural Transm 125:847–867

102. Zanotti-Fregonara P, Zhang Y, Jenko KJ et al (2014) Synthesis and evaluation of translocator 18 kDa protein (TSPO) positron emission tomography (PET) radioligands with low binding sensitivity to human single nucleotide polymorphism rs6971. ACS Chem Neurosci 5:963–971

103. Fujita M, Kobayashi M, Ikawa M et al (2017) Comparison of four 11C-labeled PET ligands to quantify translocator protein 18 kDa (TSPO) in human brain: (R)-PK11195, PBR28, DPA-713, and ER176—based on recent publications that measured specific-to-non-displaceable ratios. EJNMMI Res. https://doi.org/10.1186/s13550-017-0334-8

104. Liu B, Le KX, Park MA et al (2015) In vivo detection of age-and disease-related increases in neuroinflammation by18F-GE180 TSPO microPET imaging in wild-type and Alzheimer's transgenic mice. J Neurosci 35:15716–15730

105. Zanotti-Fregonara P, Veronese M, Pascual B et al (2019) The validity of 18 F-GE180 as a TSPO imaging agent. Eur J Nucl Med Mol Imaging 46:1205–1207

106. Gifford AN, Makriyannis A, Volkow ND et al (2002) In vivo imaging of the brain cannabinoid receptor. Chem Phys Lipids 121:65–72

107. Ahmad R, Koole M, Evens N et al (2013) Whole-body biodistribution and radiation dosimetry of the cannabinoid type 2 receptor ligand [11C]-NE40 in healthy subjects. Mol Imaging Biol 15:384–390

108. Berdyyeva T, Xia C, Taylor N et al (2019) PET imaging of the P2X7 ion channel with a novel tracer [18F]JNJ-64413739 in a rat model of neuroinflammation. Mol Imaging Biol 21:871–878

109. Dileep Kumar JS, Bai B, Zanderigo F et al (2018) In vivo brain imaging, biodistribution, and radiation dosimetry estimation of [11C]celecoxib, a COX-2 PET ligand, in nonhuman primates. Molecules 23:1–11

110. Horti AG, Naik R, Foss CA et al (2019) PET imaging of microglia by targeting macrophage colony-stimulating factor 1 receptor (CSF1R). Proc Natl Acad Sci USA 116:1686–1691

111. Narayanaswami V, Drake LR, Brooks AF et al (2019) Classics in neuroimaging: development of PET tracers for imaging monoamine oxidases. ACS Chem Neurosci 10:1867–1871

112. Fowler JS, Logan J, Shumay E et al (2015) Monoamine oxidase: radiotracer chemistry and human studies. J Label Compd Radiopharm 58:51–64